

We are IntechOpen, the world's leading publisher of Open Access books Built by scientists, for scientists

6,900

Open access books available

186,000

International authors and editors

200M

Downloads

Our authors are among the

154

Countries delivered to

TOP 1%

most cited scientists

12.2%

Contributors from top 500 universities



WEB OF SCIENCE™

Selection of our books indexed in the Book Citation Index
in Web of Science™ Core Collection (BKCI)

Interested in publishing with us?
Contact book.department@intechopen.com

Numbers displayed above are based on latest data collected.
For more information visit www.intechopen.com



Time Reversal for Electromagnetism: Applications in Electromagnetic Compatibility

Ibrahim El Baba^{1,2}, Sébastien Lalléchère^{1,2} and Pierre Bonnet^{1,2}

¹*Clermont University, Blaise Pascal University, BP 10448, F-63000, Clermont-Ferrand*

²*CNRS, UMR 6602, LASMEA, F-63177, Aubière
France*

1. Introduction

ElectroMagnetic Compatibility (EMC) is the branch of electromagnetism that studies generation, propagation and reception of involuntary electromagnetic energy in reference to the undesirable effect (electromagnetic interference) that this energy can induce. Since 1996, date of the directive 89/336/CEE (Directive 89/336/CEE, 1989) compulsory implementation concerning the electromagnetic compatibility (called CE) in Europe, and for much longer in United States, EMC has been playing an increasingly important role.

Most electrical and electronic equipment may be considered as sources of interference because it generates electromagnetic perturbations that pollute the environment and may disrupt the operation of other equipment (victims). The EMC is the ability of a device, equipment or system to operate satisfactorily within its electromagnetic environment and without producing itself an intolerable electromagnetic disturbance to anything in this environment. EMC hence controls the electromagnetic environment of the electronic equipment. To this end, EMC tackles several issues. Firstly, are the emission problems related to the generation of unwanted electromagnetic energy from a source and the measures that should be taken to reduce the generation of such disturbances and to prevent the escape of any remaining energy to the external environment. To verify that the perturbation level does not exceed a threshold value defined by standards, we measure the electric and/or magnetic fields radiated at a certain distance in the case of electromagnetic emissions, the voltage and/or current in the case of conducted disturbances. Secondly the susceptibility problems refer to the proper functioning of electrical equipment in presence of unplanned electromagnetic field. In the tests, we inject perturbation (conducting/radiating mode) on a device and check its good operation. Thirdly, for interference/noise disturbances, the EMC solutions are mainly obtained by addressing both the emissions and the vulnerability problems. This means minimizing the interference source levels and hardening the potential victims (shielding for example).

For measurements, EMC provides as test facilities different tools, the most popular are: the Anechoic Chamber (AC) (Emerson, 1973) and the Mode Stirred Reverberation Chamber (MSRC) (Corona et al., 2002; Hill, 1998). The AC is a cavity whose aim is to simulate the free space. Its walls are covered with ferrite tiles and/or polyurethane pyramids loaded with carbon absorbing electromagnetic waves and preventing their reflection. The second tool has grown in popularity over the past twenty years due to its ability to provide a

statistically uniform and homogeneous electromagnetic field on a relatively large domain (called Working Volume: WV). In addition, high field's levels could be generated in the Reverberation Chamber (RC) for relatively low injected power. For mechanical stirring, the "statistical" uniformity is mainly based on the number N of the available independent configurations (i.e. the number N of the stirrer independent positions) for the RC and the studied frequency. When the number N tends to infinity, the intern electromagnetic field properties are statistically identical from one point to another in the WV. A statistically uniform and homogeneous distribution of the field in the MSRC signifies that the same energy attacks the Equipment Under Test (EUT) from all directions and with the same polarization, when averaged over the number N of the stirrer positions. A disadvantage of the AC is the high injected power needed, thus powerful amplifier are required, in addition to the high cost of the absorbers. In comparison with the AC case, low power in MSRC is needed.

Based on the principle of reciprocity, Time Reversal (TR) is a technique that allows focusing a field in time and space. Recently, it has been applied for EMC where better results have been reported in strongly reverberant or diffracting environments. Indeed, different studies (de Rosny, 2000; Moussa et al., 2009b) in acoustics and electromagnetics have verified how RC can provide an appropriate environment for TR. One of the main advantages of the MSRC is to provide the most critical illumination of the EUT. Paradoxically, this benefit may be considered as a disadvantage, since in this case it becomes impossible to know precisely the characteristics of the electromagnetic excitation. On the one hand, recent TR studies (Cozza & Moussa, 2009; Moussa et al., 2009a) have demonstrated how to make benefit of the re-focusing to control the wave incidence and polarization attacking the EUT. On the other hand, for the same input power, the TR enables to increase the achievable field levels in the MSRC. These promising applications of TR justify its characterization in MSRC.

During susceptibility tests of electronic equipments a problem may occur when the EUT is composed of several components with different field/current threshold values that cannot be exceeded. Indeed, various immunity levels can coexist on an electronic device (power supply, components, signal integrity, etc.) or on different zones of a complex structure (automobile, aircraft, etc.) since the expected reliability might be different from an area or device to another. But, in a classical susceptibility EMC MSRC test, the illumination is statistically the same for the whole EUT placed in the working volume and it may damage components that have a smaller threshold value than the incident field. A solution consists in performing the susceptibility test independently for each component. Unfortunately, "on table" tests are not always possible and also might not represent the reality. An alternative approach can be given via TR technique and selective focusing. As a matter of fact, at the focusing time, only one component can be illuminated by a desired field level while others parts of the system are aggressed by lower noise.

In this chapter, after presenting TR basis and theoretical principles, characteristic parameters of TR are numerically studied in free space and reverberating environment before introducing an original way for performing impulsive susceptibility testing.

2. Time reversal basis

2.1 Preamble

Originally developed in acoustics (Fink, 1992) by Mathias Fink team in the early 1990 at the ESPCI (Ecole Supérieure de Physique et de Chimie Industrielles) in Paris, TR is

a physical process that is based on the principle of reciprocity. This technique allows a wave to propagate backward to its source. This retro-propagation is based on the reversibility of the wave equation in time. One of the results is to offer the possibility to focus a given wave both in time and space. Many studies have been led based on the acoustic wave equation, for applications concerning the detection and selective focusing (Prada & Fink, 1994), submarine telecommunications (Edelmann, 2005), and ultrasound and medical imaging (Quieffin, 2004) domains. More recently successful tests have been achieved in electromagnetics (de Rosny et al., 2007), mainly in telecommunications (Lerosey et al., 2004), detection and imaging (Liu et al., 2005; Maaref et al., 2008; Neyrat et al., 2008), and EMC (Davy et al., 2009; El Baba et al., 2009; 2010) fields.

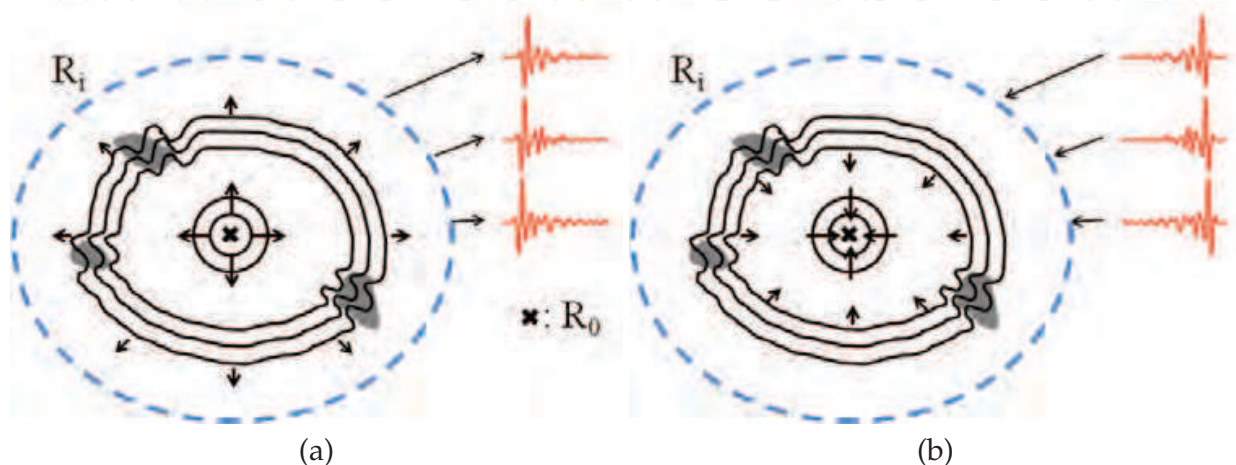


Fig. 1. (a) First and (b) second phase of time reversal process with a time reversal cavity.

In practice, the TR technique needs two phases. During the first (Fig. 1a), a source located at (R_0) emits an electromagnetic pulse that spreads in the medium. The source can be either active (transmission mode) or passive as a source of diffraction (in detection problems targets or diffusers act as passive sources). The electromagnetic radiation is recorded for a period Δt through an array of probes in reception (R_i) surrounding the source into a closed entity and forming a Time Reversal Cavity (TRC). Indeed, the data that arrive first in time travels a shorter distance than the data that arrive later. During the second phase (Fig. 1b), each probe retransmits its received signal in reversed time order, so the data that travel a longer distance are emitted earlier and the data that travel a shorter distance are emitted later (Last In First Out). Consequently, a returned wave propagates and acts as if it relives exactly its past life and this leads to a temporal and spatial focusing of the field at the original source location (R_0) where the focusing moment is considered as the time origin.

Unfortunately, from an experimental point of view and because of the large number of probes required for such operation, the TRC is not feasible. That's why classical TR experiments are conducted through a limited opening array forming the Time Reversal Mirror (TRM) (de Rosny & Fink, 2002).

In the case of a TRM, the focusing protocol by TR remains the same as in the TRC case (Fig. 2). The decrease in the angular aperture allows the convenient realization of such a mirror, but in the reemission step (Fig. 2b) only a part of the wave is time reversed leading to a loss of information reducing the focusing quality.

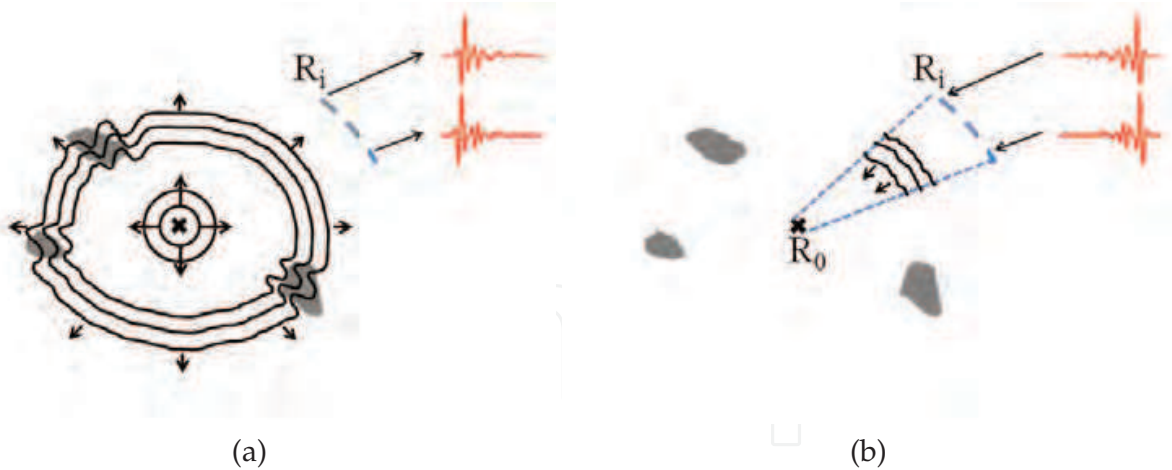


Fig. 2. (a) First and (b) second phase of time reversal process with a time reversal mirror.

This loss of information can be partially avoided if the scene takes place in a reverberant cavity. Different studies have shown that, in the case of a reverberant environment, the probe array can be replaced by a single probe (Fig. 3). Therefore, the first experiments in electromagnetism were realized in a RC. The properties of the cavity allow us to benefit from the different reflections suffered by the wave on the metal walls of the chamber, which ensures that a single probe collecting these echoes is sufficient to record necessary information for TR experiment.

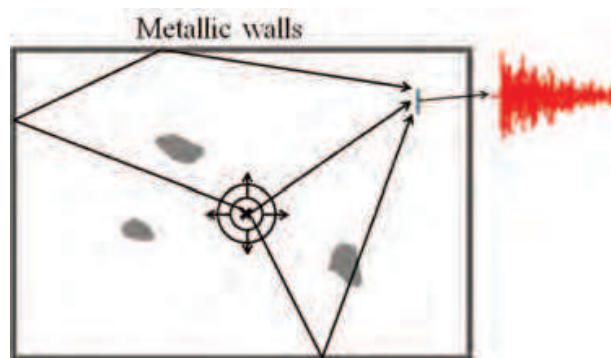


Fig. 3. TRM can be replaced by a single probe in a reverberant cavity.

2.2 Time reversal of electromagnetic waves

A propagation medium is called reversible if a field and its time reversed version can propagate in such an environment, i.e., if $\Phi(t)$ and $\Phi(-t)$ are solutions of the same propagation equation. In electromagnetism, the wave equation in a uniform and non-dissipative medium is given by

$$\frac{1}{c^2} \frac{\partial^2 \Phi}{\partial t^2} = \Delta \Phi \quad (1)$$

where Φ stands for the electric E or magnetic H field, and c is the propagation celerity of the electromagnetic waves in the medium.

Assuming that $\Phi_0(t)$ is a solution of (1), the absence of first time derivative in the left-hand side leads to the existence of another solution chronologically reversed $\Phi_1(t) = \Phi_0(-t)$.

Therefore (1) is invariant under the TR action, and theoretically, an electromagnetic scene may be replayed in reverse from time $t = \Delta t$ to $t = 0s$.

Defining the electric field estimated at the position r (given by TRM or TRC devices) and time t by $E(r, t)$, the TR data are first recorded during the experiment time $T = \Delta t$. Then, fields are returned and reemitted following a reverse chronology, for example, an electric field $E(r, t)$ is retransmitted during the reversal phase as $E(r, T - t)$, $t \in [0; T]$.

An electromagnetic wave is described by four field vectors, the electric field E , the magnetic field H , the electric induction D , and the magnetic induction B . It has been shown in (Jackson, 1998) that E and D are even vectors; however H and B are odd pseudovectors under the time reversal action. Therefore if we consider T_{TR} the time inversion operator given by $T_{TR} \{\Phi(r, t)\} = \Phi(r, -t)$, we can write

$$\begin{aligned} T_{TR} \{E(r, t)\} &= E(r, -t); & T_{TR} \{D(r, t)\} &= D(r, -t); \\ T_{TR} \{H(r, t)\} &= -H(r, -t); & T_{TR} \{B(r, t)\} &= -B(r, -t). \end{aligned} \quad (2)$$

3. Theoretical principles

An illustration of the electromagnetic TR in a reverberant environment can be obtained from Fig. 4, where R_0 is a point source representing the emission antenna, and R_i corresponds to the array of probes in reception (TRM).

The excitation pulse used is a Gaussian modulated sine pattern (Fig. 4a) emitted from the point R_0 . Probes of the TRM (R_i) record the six components of the electromagnetic fields, these signals are returned by time reversal or by the phase conjugate of their Fourier transforms (method explained in section 3.1 below) and reemitted by R_i to obtain a time and space focusing at R_0 position.

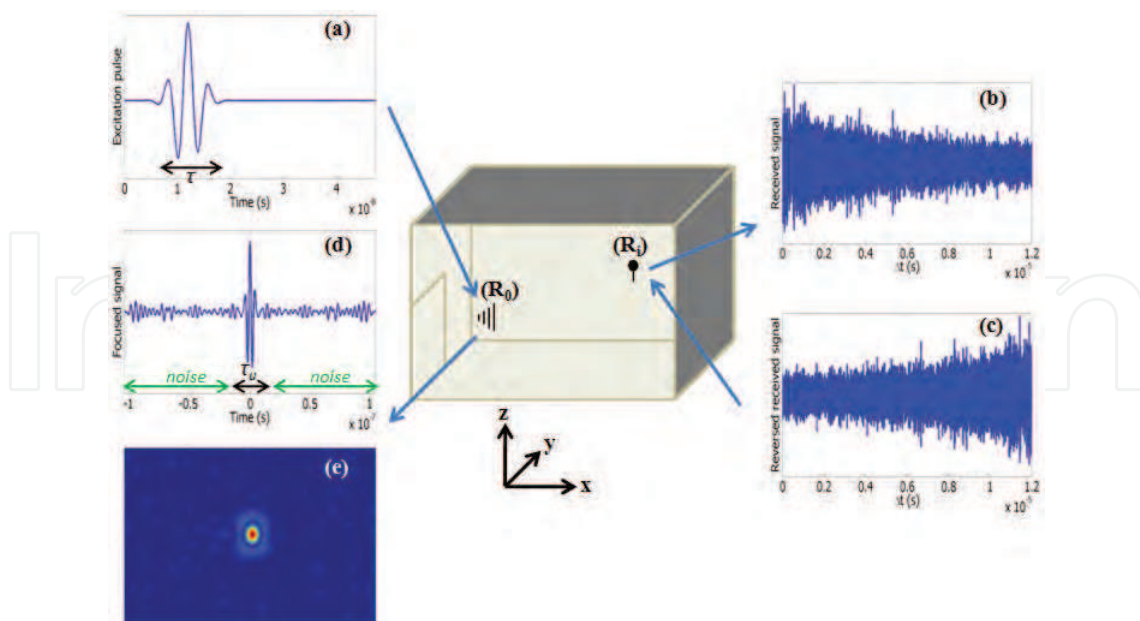


Fig. 4. TR set up, (a): excitation pulse, (b): received signal, (c): reversed received signal, (d) and (e): time and space focusing.

3.1 Time reversal and phase conjugate

Let $\tilde{\Phi}(r, \omega)$ the Fourier transform of the field $\Phi(r, t)$. It was verified that time reversing a signal corresponds to the inverse Fourier transform (FT_{inv}) of the phase conjugate of its Fourier transform

$$T_{TR} \{ \Phi(r, t) \} = \Phi(r, -t) = FT_{inv} \{ \tilde{\Phi}^*(r, \omega) \} \quad (3)$$

In Fig. 5a we plot the evolution of a signal with respect to time, and in Fig. 5b we verify that we can reverse a signal in time indifferently by the phase conjugate of its Fourier transform or by time reversal.

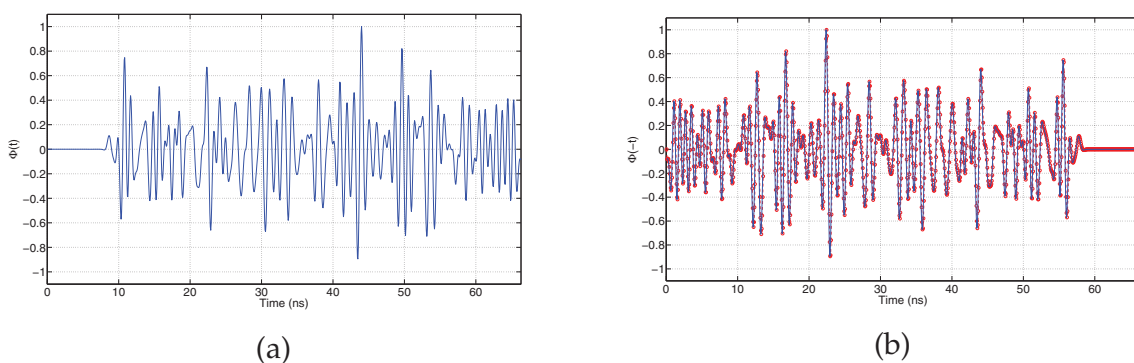


Fig. 5. (a) Temporal signal $\Phi(t)$. (b) $\Phi(-t)$ by time reversal (plain blue curve) and by inverse Fourier transform of its phase conjugate (red markers).

3.2 Mathematical foundation

The received signal (Fig. 4b) by a TRM probe (following a pulse $x(t)$ (Fig. 4a) emitted from R_0) can be written

$$y_i(t) = k(t, R_0 \rightarrow R_i) \otimes x(t) \quad (4)$$

where \otimes is the convolution product, and $1 \leq i \leq M$ with M the number of probes of the TRM, and $k(t, R_0 \rightarrow R_i)$ is the impulse response of the medium at a point R_i for a pulse emitted from R_0 . After time reversal of $y_i(t)$ (Fig. 4c) and the reemission from R_i , the focused signal on R_0 (Fig. 4d) can be written as follows:

$$E_{TR}(t, R_0) = \sum_{i=1}^M k(t, R_i \rightarrow R_0) \otimes y_i(-t) = \sum_{i=1}^M k(t, R_i \rightarrow R_0) \otimes k(-t, R_0 \rightarrow R_i) \otimes x(-t) \quad (5)$$

The advantage of working in the frequency domain is to replace the convolution product by an ordinary product. Since reversing a signal versus time corresponds to the phase conjugate of its Fourier transform, the above equation (5) takes the following form in the frequency domain

$$E_{TR}(\omega, R_0) = \sum_{i=1}^M k(\omega, R_i \rightarrow R_0) \cdot k^*(\omega, R_0 \rightarrow R_i) \cdot x^*(\omega) \quad (6)$$

Switching into matrix notation, (6) takes the following form

$$E_{TR}(\omega, R_0) = K(\omega, R_i \rightarrow R_0) \cdot K^*(\omega, R_0 \rightarrow R_i) \cdot x^*(\omega) \quad (7)$$

Now, if the medium is reversible, thanks to the reciprocity theorem, the position of a point source and a probe can be reversed without altering the field. Consequently, the impulse response from R_0 to R_i is equal to the one from R_i to R_0 , and therefore the matrix $K(\omega, R_0 \rightarrow R_i)$ is equal to the matrix $K(\omega, R_i \rightarrow R_0)$, in other words the matrix K is symmetric. In (7), the propagation matrix K is the Fourier transform of different impulse responses between one transmitter and M receivers.

3.3 Time reversal operator

One can build the so-called Time Reversal Operator (TRO) by considering the case where we have $M \times M$ transmitter receivers. The M transmitters emit successively M pulses $x_i(t) (i = 1, \dots, M)$ that can be described in the frequency domain by a vector X containing M components for each frequency. The M components given by the receivers can be written by a matrix product KX . When signals are reversed (phase conjugate in the frequency domain) and retransmitted, the resulting vector is $K^t K^* X^*$, with K the $M \times M$ propagation matrix and K^t its matrix transpose. Therefore (7) can be written

$$Foc(\omega) = K^t(\omega)K^*(\omega)X^*(\omega) \quad (8)$$

with Foc the vector containing the M focused signals for each frequency. It is interesting to note that $T(\omega) = K^h(\omega)K(\omega)$, defined as the TRO (Derode et al., 2003), is a symmetrical square matrix where h is the Hermitian conjugate (conjugate-transpose). By performing a singular value decomposition of the propagation matrix we get $K(\omega) = U(\omega)\Lambda(\omega)V^t(\omega)$, where U and V are unitary matrices and Λ is a diagonal matrix whose elements are the singular values Λ_i . On the other hand, the eigenvalue decomposition of the TRO gives $T(\omega) = V(\omega)S(\omega)V^t(\omega)$, with $S(\omega) = \Lambda^t(\omega)\Lambda(\omega)$ the diagonal matrix of eigenvalues that are the propagation matrix singular values square, and V the unit matrix of eigenvectors. This decomposition of the TRO gives us information on the propagation medium. In the detection field, Decomposition of the Time Reversal Operator (DORT) (Yavuz & Teixeira, 2006) provides information on the diffraction strength of the target via the eigenvalues and information on the position via the eigenvector of the TRO.

4. Definitions, numerical methodologies and outputs

In this study, TR is applied in a numerical way in order to facilitate its characterization in different configurations. From a practical point of view, it is easier to carry out a parametric study numerically than experimentally. For instance, a numerical study offers the flexibility to choose between a TRC and a TRM, to vary the number of probes, their positions in many test cases, etc. The proposed methodology needs to gather from the TR principles and MSRC studies. This is why the chosen method must take into account the characteristics of each domain. Indeed, it is important to consider all elements present in the experimental RC device: cavity, stirrer, equipment (Corona et al., 2002). From a numerical point of view, the influence of the metallic elements must be considered in time simulation. Consequently, the fields temporal distribution must be numerically implemented with special care given to metal facets (i.e., considered as Perfect Electric Conductor, PEC). For all the above reasons, the numerical simulations were carried out using an own-made Finite Difference Time Domain (FDTD) electromagnetic code (Bonnet et al., 2005) with E / H formulation and later for more complex cases the commercial software CST MICROWAVE STUDIO® without neglecting the fact that we can use any numerical tool that solves Maxwell's equations.

4.1 Focusing quality

To characterize time and space focusing after the TR process, we will define multiple criteria and parameters.

4.1.1 Maximum magnitude of focusing

The first idea about the quality of focusing is obtained by considering the useful part of the reconstructed signal (see duration τ_u , Fig. 4d) and implementing the absolute maximum of the focused signal.

$$\text{Max}(R_0) = \max_{t \in \tau_u} (|E_{TR}(t, R_0)|) \quad (9)$$

4.1.2 Focal spot

The second criterion characterizing spatial focusing around R_0 is the focal spot dimension (δ) which is described in two dimensions by distance along the x and y directions for which the total electric field focused at time $t = 0$ (which is the focusing time) is between $E_{TR}(R_0)$ and $E_{TR}(R_0)/2$ (in other words where $E_{TR}(R_0)/\text{Max}(R_0)$ belongs to $[-6 \text{ dB}; 0 \text{ dB}]$). The Fig. 6 illustrates this criterion in two dimensions (2-D), the principle can be extended to three dimensions (3-D). According to Fig. 6, we may write

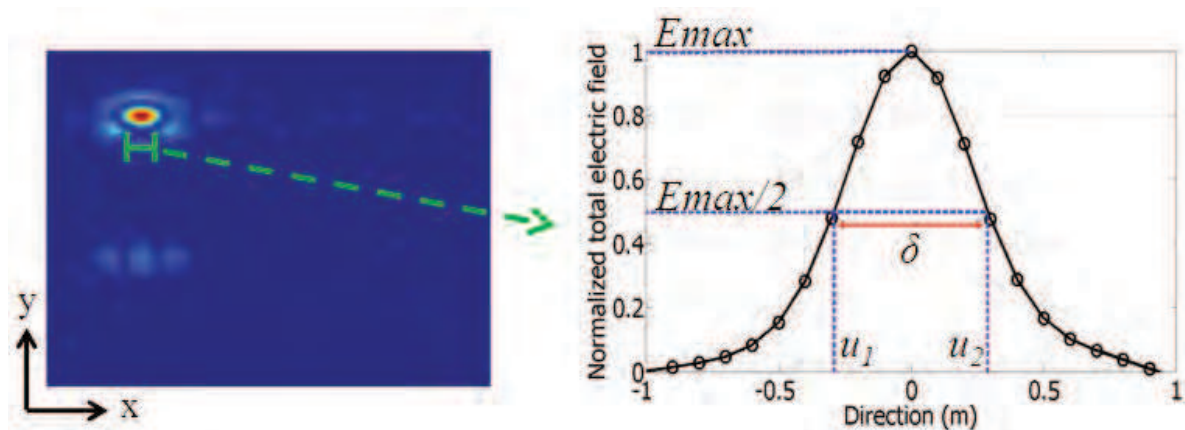


Fig. 6. Definition of the focal spot around the focusing point.

$$\begin{aligned} \delta_x &= u_{x2} - u_{x1} \\ \delta_y &= u_{y2} - u_{y1} \end{aligned} \quad (10)$$

where u_{x1} , u_{x2} , u_{y1} , and u_{y2} are the positions of both sides of R_0 at the focusing time ($t = 0$) along x and y directions. Note that the width of the focal spot in a reverberating environment, depending on the diffraction limit, is about $\lambda/2$ where λ is the wavelength corresponding to the frequency of the excitation pulse. On the other hand, in free space the focal spot is given by the following formula

$$\delta = \frac{\lambda F}{D} \quad (11)$$

with F the distance between the focusing point (R_0) and the TRM (R_i), and D the size of the TRM.

4.1.3 Signal to noise ratio

An important criterion to characterize focusing in a reverberation chamber is the Signal To Noise (*STN*) ratio, which was theoretically introduced in (de Rosny, 2000) as follows:

$$STN \cong \frac{4\sqrt{\pi}\Delta H\Delta\Omega}{\frac{\langle\alpha\rangle^4}{\langle\alpha^2\rangle^2} + \frac{\Delta H}{\Delta t}} \quad (12)$$

where we have: $\Delta\Omega$, the frequency bandwidth of the excitation pulse; α , the ensemble average of the eigenmodes magnitude of the chamber; ΔH , the Heisenberg's time given by the following formula

$$\Delta H = 2\pi n(\omega) \quad (13)$$

with $n(\omega)$, the average modal density of the reverberation chamber assumed constant over the entire bandwidth $\Delta\Omega$.

Numerically, this ratio can be calculated from the temporally focused signal in R_0 , and it is known as the temporal *STN* ratio (STN_t) which is the ratio between the squared magnitude of the focused signal peak (Fig. 4d, $t = 0$) and the temporal noise around the peak. It is defined as the square of the focused field RMS on a part of the simulation time apart the useful signal (Fig. 4d, $t \notin \tau_u$).

The ratio is given by

$$STN_t = \frac{\langle E_{TR}(r = R_0, t = 0) \rangle^2}{\langle E_{TR}^2(r = R_0, t \notin \tau_u) \rangle} \quad (14)$$

where $E_{TR}(R_0, t)$ represents the focused total electric field in R_0 .

Similarly to (14), we can also calculate the spatial *STN* ratio (STN_s) which is the ratio of the squared magnitude of the focused signal peak in R_0 on the square of the field RMS value calculated over the rest of the studied domain at the focusing time ($t = 0$), this one can be considered as "spatial noise". So we have

$$STN_s = \frac{\langle E_{TR}(r = R_0, t = 0) \rangle^2}{\langle E_{TR}^2(r \neq R_0, t = 0) \rangle} \quad (15)$$

It has been proved in (Moussa et al., 2009a) that for whole averages and as RC are ergodic systems, temporal *STN* ratio is equivalent to spatial one. In what follows, for the sake of simplicity, both temporal and spatial signal to noise ratios are denoted *STN*.

4.1.4 Delay spread

To characterize the temporal focusing (and linked to spatial aspects) in reverberation chamber, the delay spread parameter is defined as in (Ziadé et al., 2008). Indeed, the impulse response shown in Fig. 4b shows that a pulse emitted from a source will be received as a series of pulses (with different arrival times). This parameter stands for time separating last echo and straightforward way. The root mean square of the delay spread parameter (linking the standard deviation of time with the mean value) can be written for the E fields by

$$\tau_{RMS} = \sqrt{\frac{\int (\tau - \tau_m)^2 |E_{TR}(\mathbf{r}, \tau)|^2 d\tau}{\int |E_{TR}(\mathbf{r}, \tau)|^2 d\tau}} \quad (16)$$

with τ_m : mean value of E delays. Electric fields E_{TR} are given at location r and time τ . Thus, the average delay τ_m is given by

$$\tau_m = \frac{\int \tau |E_{TR}(\mathbf{r}, \tau)|^2 d\tau}{\int |E_{TR}(\mathbf{r}, \tau)|^2 d\tau}. \quad (17)$$

4.2 FDTD method for time reversal

In the FDTD method, Maxwell's equations are discretized following the Yee algorithm (Yee, 1966), these equations are invariant to time reversal transformation (Jackson, 1998). For more simplicity, we will consider here a 2-D formulation; the 3-D case can be straightforwardly extended by simple modifications. In the FDTD method, electric and magnetic fields are calculated by an explicit "leapfrog" scheme for time intervals separated by a half time step, in other words from the electric field at time $t = n - 1/2$ and the magnetic field at time $t = n$, the electric field at time $t = n + 1/2$ is calculated as we can see in the discretized Maxwell's equation below (18) (2-D TM mode)

$$E_z^{n+1/2} \left(i + \frac{1}{2}, j + \frac{1}{2} \right) = \frac{2\epsilon - \sigma dt}{2\epsilon + \sigma dt} E_z^{n-1/2} \left(i + \frac{1}{2}, j + \frac{1}{2} \right) + \frac{2dt}{2\epsilon + \sigma dt} \times \left[\frac{H_y^n \left(i + 1, j + \frac{1}{2} \right) - H_y^n \left(i, j + \frac{1}{2} \right)}{dx} - \frac{H_x^n \left(i + \frac{1}{2}, j + 1 \right) - H_x^n \left(i + \frac{1}{2}, j \right)}{dy} \right] \quad (18)$$

where dx , dy and dz are the space steps in Cartesian directions (Ox), (Oy), and (Oz), while dt is the time step. σ and ϵ represent conductivity and permittivity of the medium.

Regarding time reversal, we need to reverse the calculation sequence. In fact, the electric field at time $t = n - 1/2$ is calculated from the electric field at time $t = n + 1/2$ and the magnetic field at time $t = n$. To do that, we only need to take the discretized Maxwell's equations and rewrite them under the desired shape (Sorrentino et al., 1993)

$$E_z^{n-1/2} \left(i + \frac{1}{2}, j + \frac{1}{2} \right) = \frac{2\epsilon + \sigma dt}{2\epsilon - \sigma dt} E_z^{n+1/2} \left(i + \frac{1}{2}, j + \frac{1}{2} \right) - \frac{2dt}{2\epsilon - \sigma dt} \times \left[\frac{H_y^n \left(i + 1, j + \frac{1}{2} \right) - H_y^n \left(i, j + \frac{1}{2} \right)}{dx} - \frac{H_x^n \left(i + \frac{1}{2}, j + 1 \right) - H_x^n \left(i + \frac{1}{2}, j \right)}{dy} \right] \quad (19)$$

The above relation (19) should be applied to calculate fields at earlier moments from the later instants. To check the validity of this TR algorithm, consider a 2-D domain whose boundaries are simulated by PEC. An excitation point source emitting a Gaussian pulse is located in the middle of the Computational Domain (CD). The field propagates in the domain for a time $t = t_1$. Fig. 7a shows the distribution of the electric field E_z at time $t = t_1$. For $t > t_1$, time is reversed and we consider the field distribution E_z at time $t = t_1$ (Fig. 7a) as initial condition. After this time, and from the modified FDTD equations, we come to rebuild the field distribution of the source and found its position (Fig. 7b). This TR algorithm was effectively applied in (Neyrat, 2009) for buried object detection.

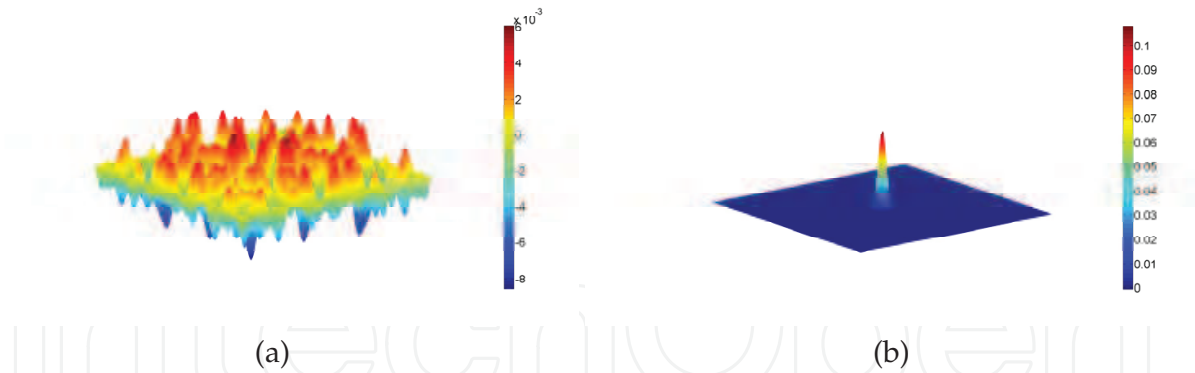


Fig. 7. (a) Electric field E_z distribution at time $t = t_1$. (b) Reconstructed pulse obtained by inverse FDTD simulation.

The technique described above may only have numerical applications since fields have to be recorded for each discretisation point. In our case (applying TR in EMC), our objective is not detection, but focusing field numerically in a given place and time, and for instance, extending to experimental developments in further works. To avoid field registration throughout the whole domain which should be impossible experimentally, we will focus on the technique briefly described on Fig. 4. In this case, the field is recorded on probes during the first phase using the FDTD discretization (18), and in the second it is time reversed and retransmitted without changing the Maxwell's equations in the FDTD code. This alternative is the one used in most of TR experiments and TR numerical simulations.

4.3 Numerical configurations

Already mentioned, simulations were performed using an own-made code based on the FDTD method. Two CDs were considered: the first one is a 2-D TM mode given by $CD_1 = 3.3 \times 3.3 \text{ m}^2$, the second is a 3-D $CD_2 = 2.2 \times 1.5 \times 1 \text{ m}^3$ volume. The excitation signal used for the first phase of the TR process is a Gaussian modulated sine pattern (Fig. 8a)

$$x(t) = E_0 e^{-\left(\frac{t+\frac{z-z_0}{c}-t_0}{\ell}\right)^2} \sin(2\pi f_c t) \quad (20)$$

where E_0 is the Gaussian magnitude, z_0 and t_0 are respectively the delays with respect to the origins of space and time, ℓ is the mid-height width of the pulse, and f_c is the central frequency.

The bandwidth $\Delta\Omega$ of this pulse is the frequency distance (Fig. 8b) of both sides of the central frequency with respect to the attenuation (Att) of the maximum amplitude (the amplitude corresponding to f_c). To calculate $\Delta\Omega$, we consider successively different attenuation levels. For instance, in the case of $Att = 2$ (corresponding to a -6 dB decrease) we divide the amplitude corresponding to f_c by 2 and calculate f_2 and f_1 , and the bandwidth is given by $\Delta\Omega = f_2 - f_1$.

For all FDTD simulations in this chapter, we used a Gaussian modulated at a central frequency $f_c = 600 \text{ MHz}$ and bandwidth $\Delta\Omega = 350 \text{ MHz}$ calculated at -6 dB . Simulations are performed with a uniform spatial discretization $dx = dy = 3.3 \text{ cm}$ for the 2-D domain, and $dx = dy = dz = 3.3 \text{ cm}$ for the 3-D domain (corresponding to $\lambda_{f_c}/15$, λ_{f_c} : wavelength corresponding to the central frequency f_c).

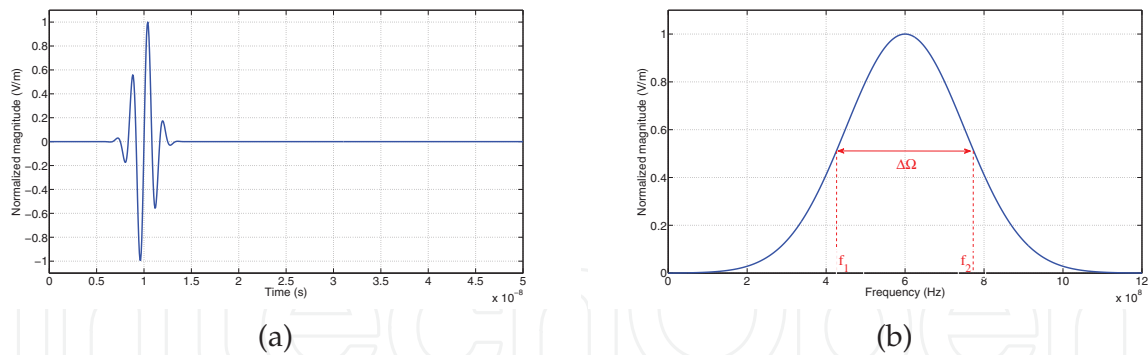


Fig. 8. (a) Time response of the excitation signal used for the first phase of TR and (b) its spectrum.

5. Numerical results

In this section, we investigate the impact of various parameters on the TR process. These will be studied initially in free space, then we will see how the complexity of the environment can improve the focusing quality, and finally we will check how reverberant media are ideal environments to work with TR.

5.1 Preliminary study in free space

The first numerical example treated helps to qualify focusing relatively to the number of probes in the TRC. For this, we consider the 2-D CD_1 domain (Fig. 9) where the excitation source is located in the middle of the area and a TRC composed of 320 probes completely surrounding the point source. Free space is simulated by Mur absorbing boundary conditions (Mur, 1981).

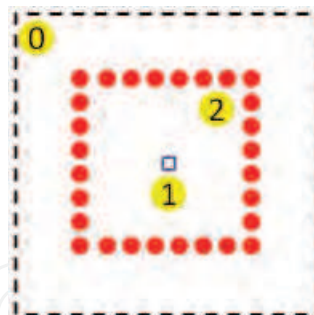


Fig. 9. CD_1 domain: (0) absorbing conditions, (1) source R_0 , (2) TRC probes R_j .

A 7 ns pulse (Fig. 8a) is emitted from the point source and the TRC probes record the evolution of the electric field component E_z and the magnetic field components H_x and H_y (TM mode). After time reversal and reemission of the recorded signals by the TRC probes, we can find the position of the excitation source as shown in the spatio-temporal evolution of the absolute value of the electric field E_z on Fig. 10.

The returned excitation signals $x(-t)$ and the normalized temporal focusing signal E_{TR} at the point source are plotted on Fig. 11a. The original shape of the excitation signal and the position of the emission point are observed (here it is an active source but it can also be a diffracting object).

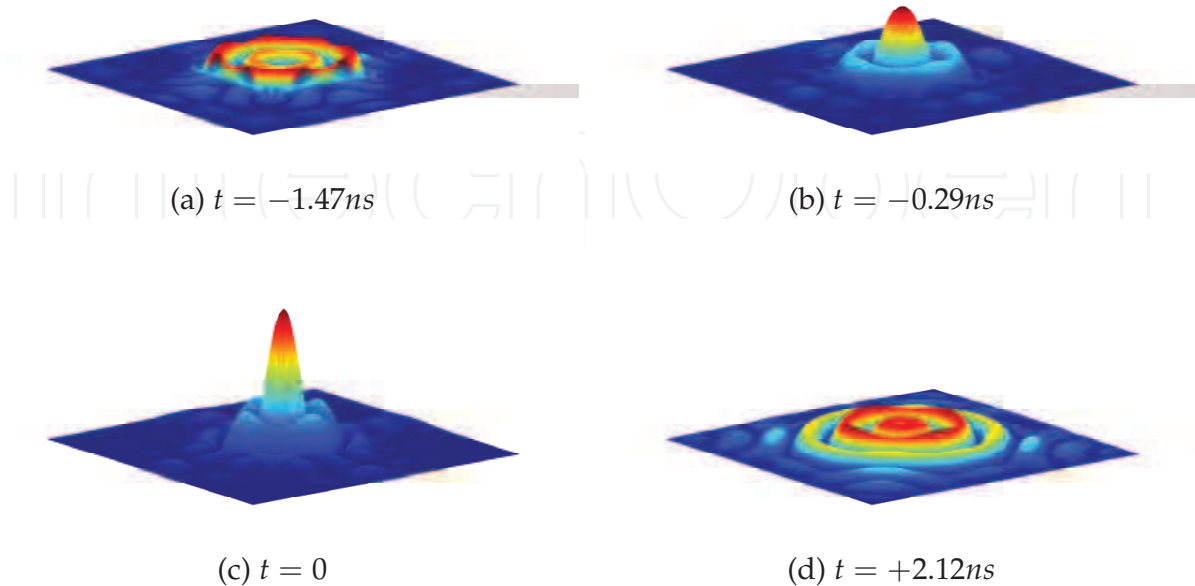


Fig. 10. Electric field spatio-temporal evolution around focusing point (focusing time set as time origin).

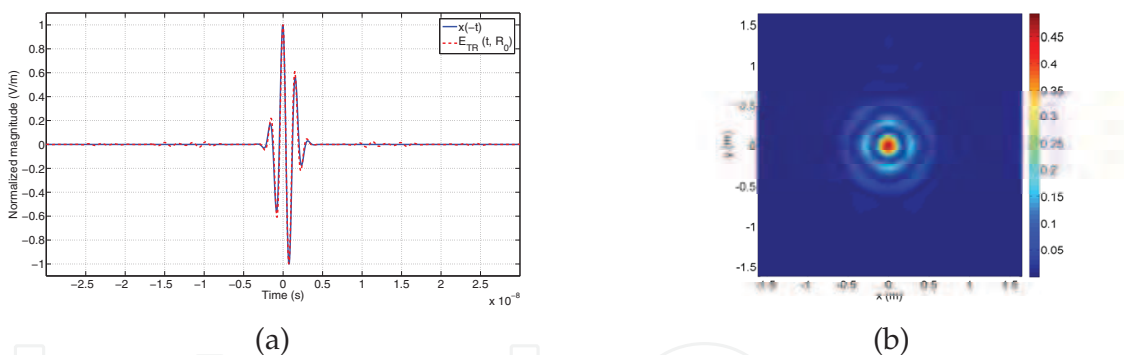


Fig. 11. (a) Temporal and (b) spatial focus on the point source at focusing time ($t = 0$).

The number of probes used in the previous example (320 probes) is the maximum number allowed by the used FDTD discretization. In Fig. 12a, curves (1), (2) and (3) demonstrate the importance of the probes number in the TRC on the maximum magnitude of focusing criterion. In addition, we note (Fig. 12b) that this criterion increases linearly with the number of probes.

For a 3-D domain (CD_2), two cases were treated. The first one deals with an excitation emitted by the point source along the three components of the electric field E_x , E_y and E_z , and the second one only E_x component is considered. The Fig. 13 shows the treated numerical configuration where the excitation point is in the middle of the CD_2 (Cartesian coordinates $(0, 0, 0)$ which corresponds to the mesh $(34, 23, 15)$, and the TRC is composed of 6114 probes corresponding to the maximum number allowed by the used FDTD discretization.

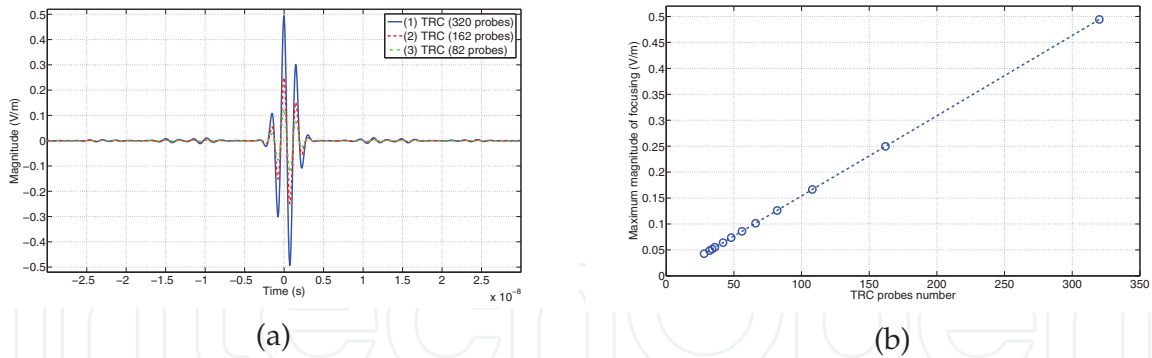


Fig. 12. (a) Focused signals ($E_{TR}(t, R_0)$) for different number of probes uniformly distributed on the TRC. (b) Maximum magnitude of focusing criterion with respect to the TRC probes number.

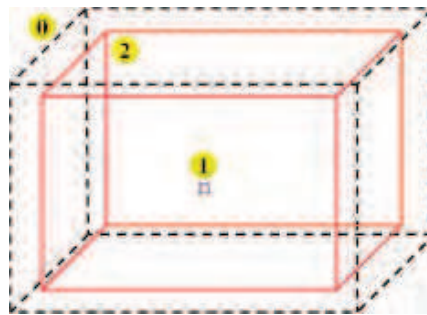


Fig. 13. CD_2 domain: (0) absorbing conditions, (1) source R_0 , (2) TRC.

In the first case, we can see that the focused signal after TR is along the three polarizations x , y and z (Fig. 14a), and we can focus on the spatial distribution of the total electric field at focusing time (Fig. 14b) where an energy concentration appears around the point source.

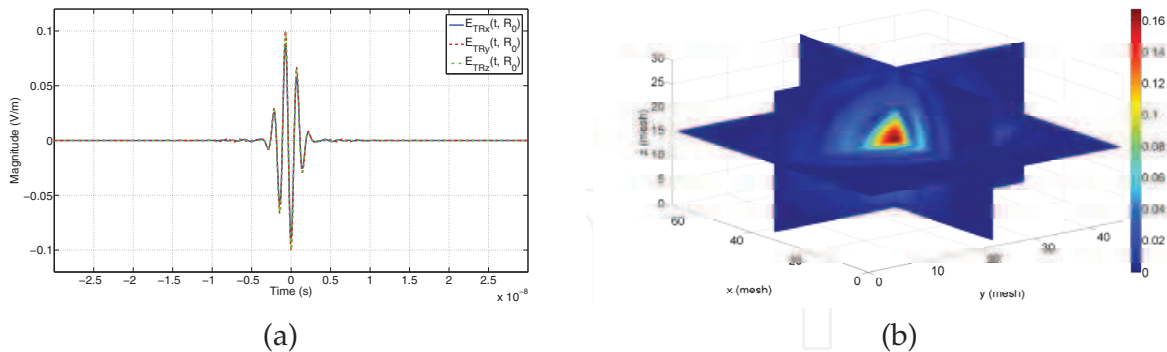


Fig. 14. (a) Time focusing for emitted excitation along E_x , E_y , and E_z . (b) Total electric field cartography at focusing time ($t = 0$).

In the second case (where the excitation is along E_x), we see that the electric field is focused only along the x component (Fig. 15) and this can be verified if we extract E -field over a plan corresponding to $z = 0$ and we look to the field cartography at focusing time for all polarizations (Fig. 16). We clearly note that the electric field corresponding to E_y and E_z is almost zero compared to E_x .

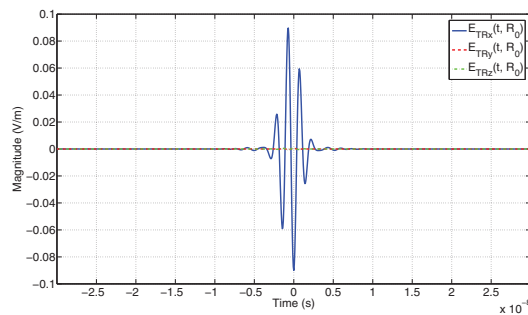


Fig. 15. Time focusing for excitation emitted along E_x .

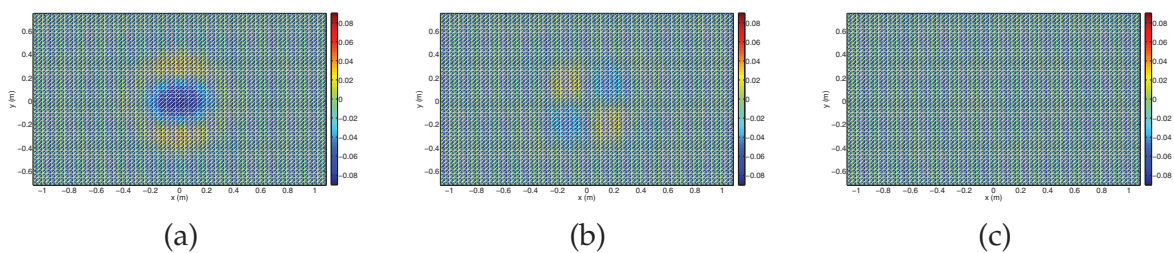


Fig. 16. E -field slice plan corresponding to (a) E_x , (b) E_y , and (c) E_z components at the focusing time ($t = 0$).

We deduce that it is theoretically possible to control the polarization of the wave attacking the EUT without changing the antenna polarization. This application can be very interesting especially in a reverberant environment, as we shall see later in this chapter.

Given the huge number of probes needed for the TRC and the inability to achieve such an experimental configuration, in the following simulations TRC is replaced by a TRM with limited opening (Fig. 17).

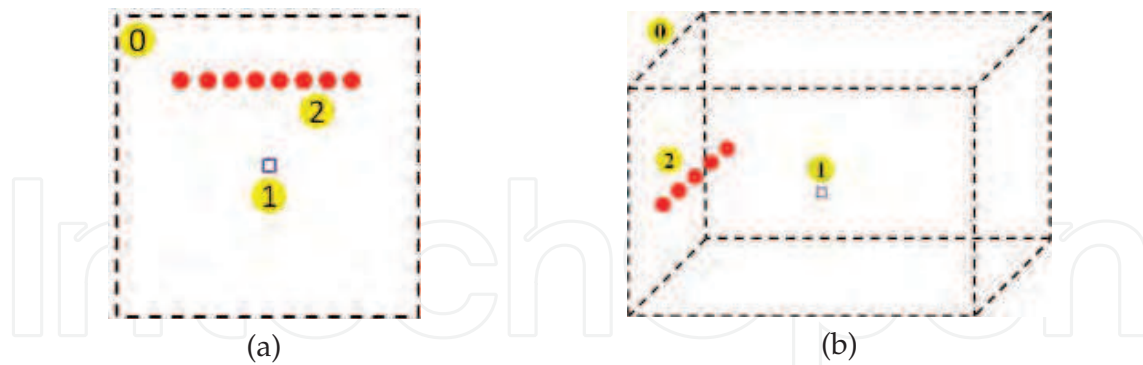


Fig. 17. (a) CD_1 and (b) CD_2 domains: (0) absorbing conditions, (1) source R_0 , (2) TRM probes R_i .

The previous simulations are repeated with a TRM of 41 probes for 2-D domain and 54 probes for 3-D domain, comparing temporal focusing (Figs. 18a, 19a) with those obtained with a TRC (Figs. 12a, 14a), we note that the maximum magnitude of focusing is greatly reduced. Moreover we note a spatial focusing damage. The Figs. 18b and 19b show that focusing is of weaker quality comparatively to TRC cases (Figs. 11b, 14b).

So, unlike the previous case, recording fields on one side of the domain can not reconstruct the exact propagation of the wave as it spread, from the fact that the information is reduced

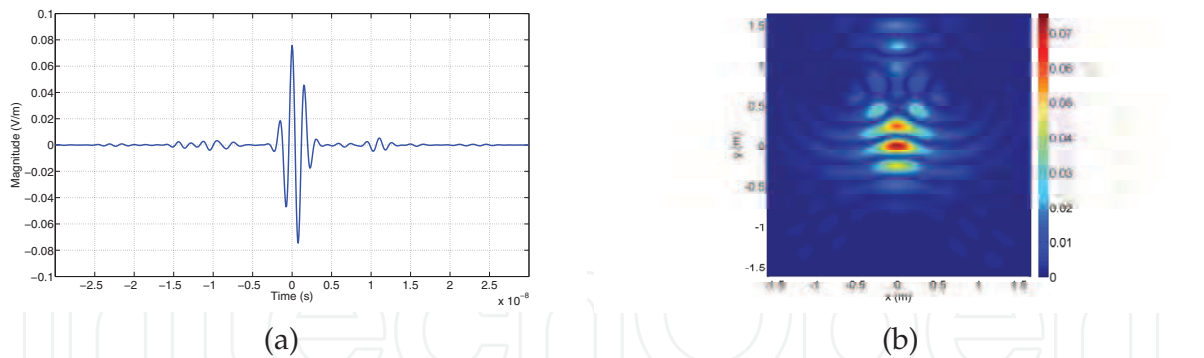


Fig. 18. CD_1 : (a) Temporal and (b) spatial focusing on the point source at the focusing time ($t = 0$) using a TRM.

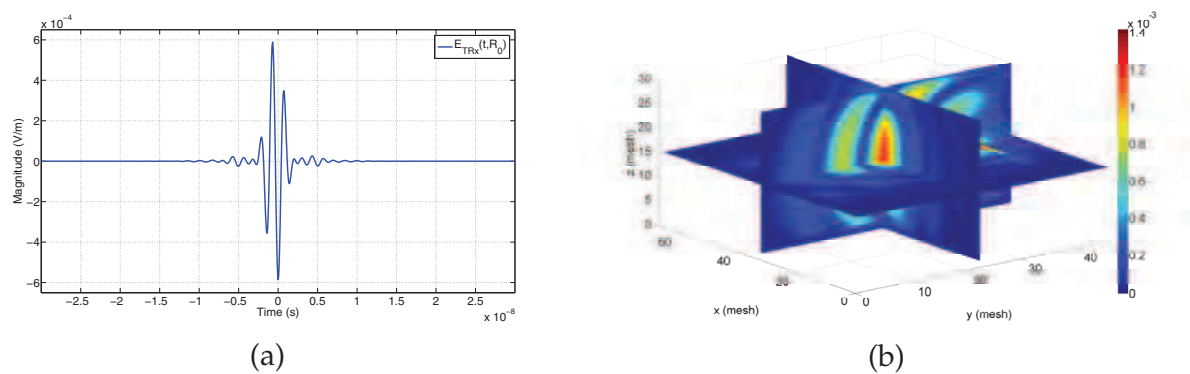


Fig. 19. CD_2 : (a) Temporal and (b) spatial focusing on the point source at the focusing time ($t = 0$) for an excitation along E_x , E_y , and E_z using a TRM.

especially for 3-D. This loss of information can be solved by making the domain more complex, which will allow recording more information without increasing the number of TRM probes. In the following, we will only consider the 3-D domain (CD_2).

5.2 Introducing multiple reflections

To collect more information on the wave propagation in the first phase of TR, it is better to increase the TRM angular opening or make the environment more complex. To achieve this, a metal plate modeled by PEC is added in the domain (Fig. 20).

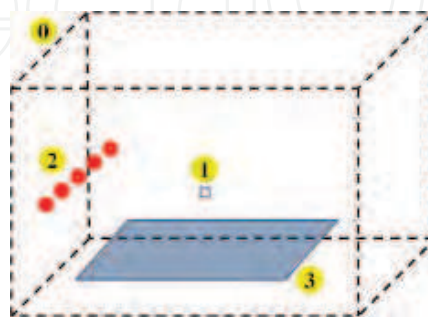


Fig. 20. CD_2 domain: (0) absorbing conditions, (1) source R_0 , (2) TRM probes R_i , (3) metallic plate.

The goal here is to take advantage of reflections due to the presence of the metal plate. The Fig. 21a confirms the expectation about the presence of a diffracting object: we see that the signal received by a probe of the TRM (component x of the electric field E_x) in a complex environment contains more information. Indeed, the waves due to the PEC reflections improve the maximum magnitude of focusing (Fig. 21b).

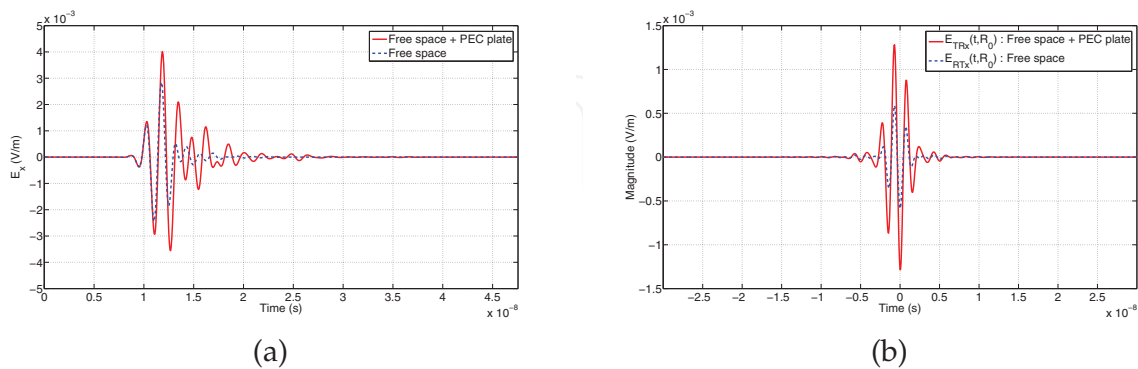


Fig. 21. (a) Electric field E_x received by a TRM. (b) The temporal focusing on the source point in both cases (free space + metallic plate and free space) for an excitation along E_x , E_y , and E_z using a TRM.

Following this idea, we can easily imagine that suitable media to apply the TR are the reverberating environments, supporting the interests of its application in the MSRC. Indeed, the multiple reflections suffered by the wave on the metal walls of the chamber will allow us to replace the TRM by a limited number of probes.

5.3 Time reversal in a reverberant environment (reverberation chamber)

In this section, the previous configuration CD_2 is preserved with a 8-probes TRM and excitations along E_x , E_y and E_z . The purpose of this part is to show the benefits of TR application in the MSRC across different test cases:

- the "free space" data will be compared to a reverberant environment,
- the duration of the TR window, in other words duration of the reversed signal, is studied looking the STN ratio and the link with the modal density of the chamber,
- intrinsic properties of the wave propagation in the cavity will be treated by focusing on the randomness of the probes location,
- and finally, we will study the influence of the excitation source parameters in terms of the focal spot size.

5.3.1 Comparison with free space

The presence of perfectly metallic boundary conditions replacing absorbing conditions implies that the impulse response (Fig. 22a) received by one of the 8 probes of the TRM is composed of several reflections that never decrease, unlike free space case (Fig. 21a). It is important to note that real losses are not included in this section. As a result, the numerical energy injected after time reversal appears comparatively higher in RC than with absorbing conditions. This improves the focusing quality in terms of maximum focusing magnitude: 6.10^{-4} V/m with 51 probes as TRM in free space (Fig. 19a) and 0.04 V/m with a TRM of 8 probes in RC (Fig. 22b).

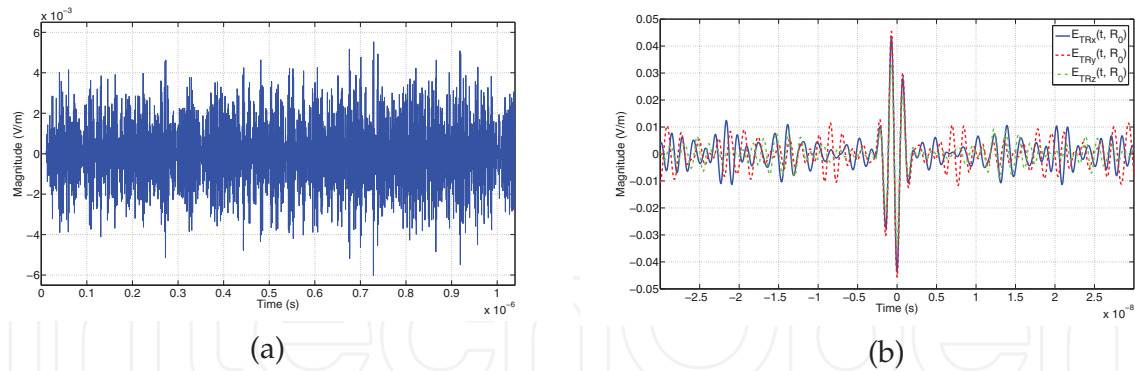


Fig. 22. (a) Electric field E_x received by a probe of the TRM in RC. (b) Temporal focusing by TR in RC.

To investigate the spatial focusing by studying the focal spot size in all directions and check the temporal focusing using the delay spread criterion (τ_{RMS}), we recorded the total electric field around the focusing point along x , y and z axis. On the one hand, results given in Fig. 23a show that focusing is symmetrical and is $\lambda_{f_c}/2$ order (dimension of the focal spot = $0.25 \text{ m} = \lambda_{f_c}/2$).

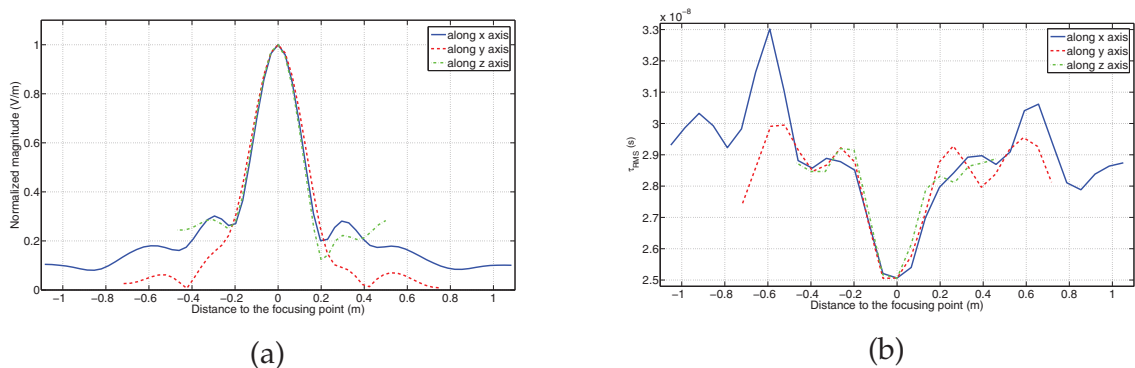


Fig. 23. (a) Total electric field ($E_{TR}(r, t = 0)$) and (b) delay spread (τ_{RMS}) with respect to the distance to the focusing point.

On the other hand in Fig. 23b, the delay spread criterion is implemented. Indeed, the signals are sent back on the principle of first wave arrived last broadcast, so that all waves arrive simultaneously at the focusing point. The criterion τ_{RMS} measures the arrival time between first and last wave. Therefore, the smaller this parameter is over a given point in space, better the focusing is (in terms of agreement between time and space). For this we can see in Fig. 23b the smallest value of τ_{RMS} (along x , y , and z axis around R_0) corresponds to the point source. This means that TR has reduced the echoes and the excitation pulse was reconstructed even if we are in a reverberant environment.

The last studied parameter in this section is the propagation matrix K (section 3.3). This matrix can be constructed numerically in a simple way. To do this, an array of 24 point sources ($i = 1$ to 24) separated by 23 cm from each other is placed on one side of the domain and the same number of probes ($j = 1$ to 24) is used on the other side. We measure the 576 inter-element impulse responses ($k_{ij}(t)$) in both free space and RC. After a Fourier transform of each $k_{ij}(t)$, the propagation matrix K is known to the whole spectrum of the excitation pulse. For each frequency a singular value decomposition is applied. The singular values

of K in both cases are shown in Fig. 24. Note that in the case of RC the number of singular values is much more representative than the free space case so the matrix K has a higher rank. For the central frequency $f_c = 600 \text{ MHz}$, we see that we have 20 singular values for the RC case and only 5 in free space (with a -32 dB threshold relatively to the first singular value). Physically the number of significant singular values is approximately the number of independent probes whose recorded impulse responses are not correlated, which is a crucial point in the application of TR in a reverberant environment, as we will see later in this chapter.

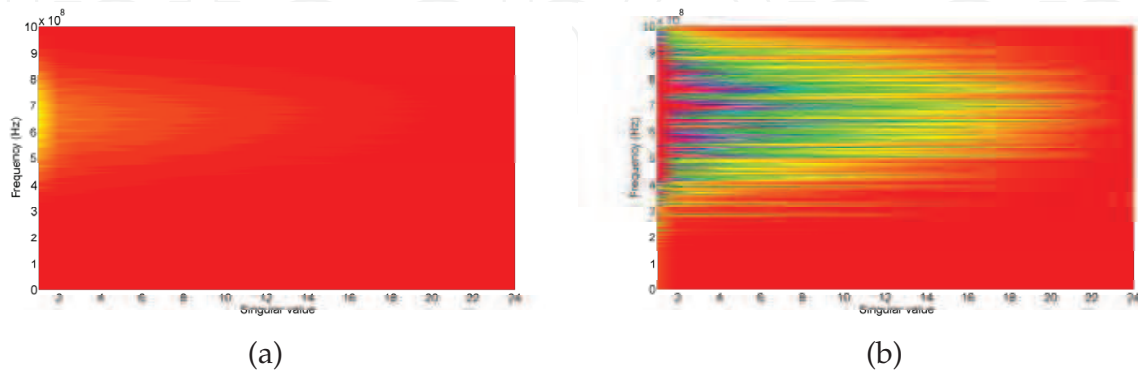


Fig. 24. Singular value decomposition of the propagation matrix K in (a) free space and (b) RC.

5.3.2 Influence of simulation duration

To study the influence of the reversed signal duration, in other words, the influence of the simulation duration on the STN ratio, different numerical tests were processed by varying the duration Δt and conserving one probe as TRM. To see more representative average data, each simulation of the second phase of TR is repeated nine times and at each time the receiving probe is placed in a different position of the chamber.

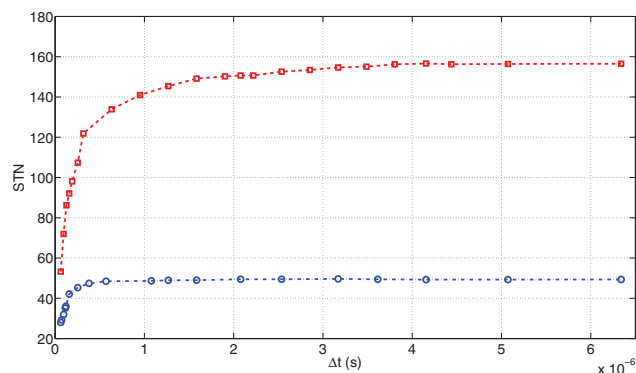


Fig. 25. STN ratio with respect to simulation duration (case 1: $f_c = 400 \text{ MHz}/\Delta\Omega = 260 \text{ MHz}$: blue circles markers, case 2: $f_c = 800 \text{ MHz}/\Delta\Omega = 260 \text{ MHz}$: red squares markers).

On Fig. 25, we plotted for each studied case the STN ratio, numerically calculated from (14), averaged over the nine positions of the TRM probe, with respect to the simulation duration Δt . We note that the STN ratio increases with the central frequency of the excitation signal, also this ratio becomes stable after a given time called Heisenberg time (ΔH). From (13), where $n(\omega)$ is deduced numerically by counting the resonant modes in the bandwidth (see later

in this section), we obtain the Heisenberg time value. These results are verified numerically in Fig. 25 (e.g. in case 1, the Heisenberg time value $\Delta H = 0.3 \mu s$ given by (13) is verified numerically).

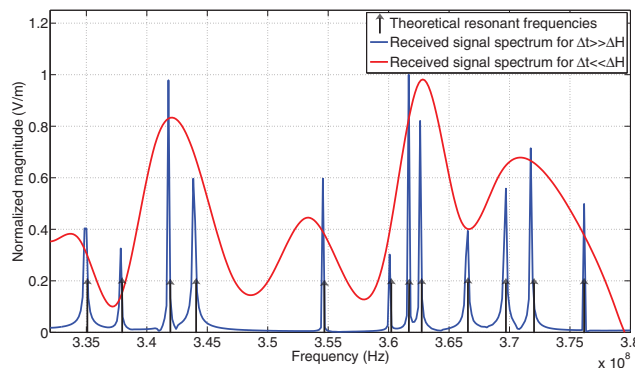


Fig. 26. Impulse response spectrum.

This behavior of *STN* saturation has been experimentally explained in terms of "information grains" and used in (de Rosny, 2000). In this model the impulse response of the system with $1/\tau$ as frequency width (τ : time duration of the modulated Gaussian), can be linked to a succession of uncorrelated information grains whose frequency width is around $1/\Delta t$. From Fig. 26, we see that the *STN* saturation seems to be a consequence of the existence of a finite number of resonant frequencies in the impulse response spectrum. Thus, for short time simulation durations, one information grain covers several frequencies (eigenmodes of the chamber). In this case, the number of information grains is equal to $\Delta t/\tau$, and the *STN* ratio increases with time. However, for longer durations, the number of information grains that can not be set only on the resonance frequencies stabilizes (number of information grains is equal to $1/(\tau\delta f)$ with δf : average distance between two successive eigenmodes); all the frequencies of the chamber are being resolved. The *STN* ratio becomes independent of the simulation duration (Fig. 25). This was predicted by the theoretical formula of *STN* ratio (12).

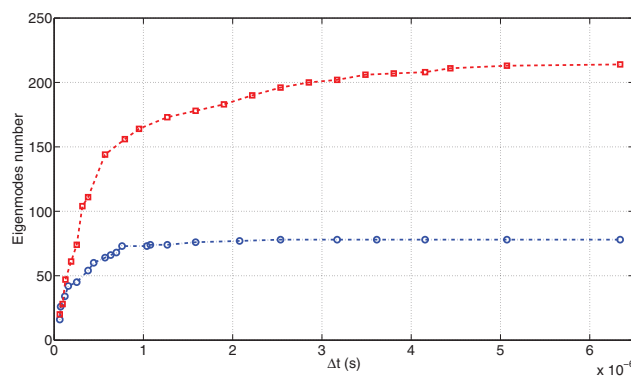


Fig. 27. Eigenmodes number with respect to simulation duration (case 1:

$f_c = 400 \text{ MHz}/\Delta\Omega = 260 \text{ MHz}$: blue circles markers, case 2:

$f_c = 800 \text{ MHz}/\Delta\Omega = 260 \text{ MHz}$: red squares markers).

This ratio depends on the product $\Delta H\Delta\Omega$ which is simply the number of eigenmodes. Thus Fig. 27 illustrates this saturation phenomenon: the evolution of the eigenmodes number of the RC in the bandwidth $\Delta\Omega$ is plotted as a function of simulation duration. The direct

estimation of the number of resonance modes from Weyl theoretical formula (Liu et al., 1983) does not take into account the numerical characteristics of temporal simulation. As such, the eigenmodes number is defined from the mean total electric field spectrum recorded by the nine positions of the receiving probe: numerical calculation is achieved by counting the resonance peaks in the spectrum (Fig. 27). Note that the eigenmodes number stabilizes for duration greater than the corresponding Heisenberg time, which verifies the saturation of the *STN* ratio (Fig. 25).

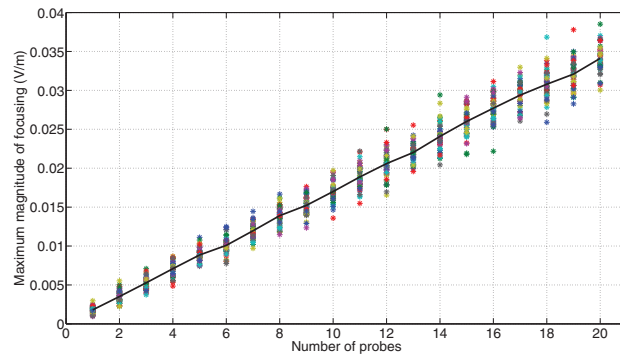
5.3.3 Contribution of random receivers locations and number

Arnaud Derode has proved in (Derode et al., 1999) that the *STN* ratio increases with the root of the number of used probes, and this is caused by the fact that each supplementary probe brings an additional information uncorrelated with known information. In the RC case, uncorrelated information are the eigenmodes of the chamber. To study the influence of probe number in the TRM on the *STN* ratio, Various FDTD simulations are achieved for the case where $f_c = 400 \text{ MHz}$ and $\Delta\Omega = 260 \text{ MHz}$ using different numbers of probes (from 1 to 20) located randomly inside the CD (except on source and PEC boundaries). In order to compute mean values of outputs, each previous experiment is repeated 50 times for each number of probes (i.e. 50 random draws following a uniform law for 1 probe, then 50 for 2 probes, ...). We chose a TR window $\Delta t = 65 \text{ ns}$ much smaller than the corresponding Heisenberg time ($\Delta H = 300 \text{ ns}$).

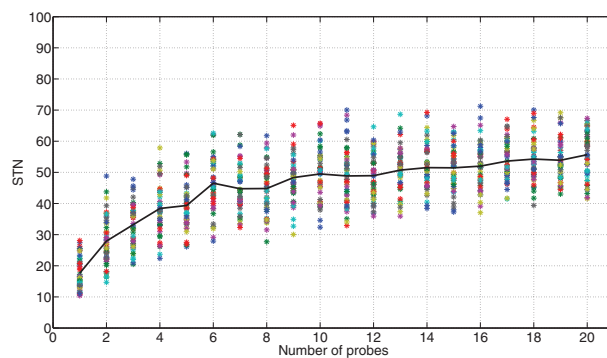
The Fig. 28a shows that the maximum magnitude of focusing increases linearly with the number of probes. Contrary to maximum output, the use of *STN* criterion (more representative for a RC studies according to multiple reflections on PEC and thus to multiple sources) seems more relevant to characterize the quality of focusing. From the Fig. 28b (results obtained from the temporal *STN* ratio) and assuming a given number np of receiving probes ($np \cong 8$ or 9), focusing may appear independent from the probes number and the *STN* ratio stabilizes and does not follow the root law observed in (Derode et al., 1999). Indeed, after an increase, the *STN* ratio shows a level of saturation and the mean trend seems to reach a limit as a function of the probes number (from 10 to 20 probes in this case). This is due to the fact that the new probes do not provide any additional information since the eigenmodes of the RC are already resolved. To a weaker extent, the positions of the receiving probes need particular care. This result may provide great interests for MSRC studies since it is far more convenient to repeat some measurements using less probes for a given time than multiplying the number of field sensors for a shorter duration. Obviously, taking advantage of multiple scattering in RC, the use of a single TR probe needs a sufficient time of experiment to provide enough information (in comparison with a multi-probes setup).

5.3.4 Spatial resolution

In EMC tests, sometimes we need to obtain a field distribution following a focal spot as small as possible. In order to study the influence of the excitation pulse parameters in the focal spot, we computed the normalized total electric field as a function of the distance to R_0 along x axis by varying the central frequency and the bandwidth of the modulated Gaussian. We note (Fig. 29) that the size of the focal spot (as defined in section 4.1.2) decreases by increasing the central frequency and the bandwidth of the excitation pulse. Our interest is, for TR experiences in RC, to increase f_c and $\Delta\Omega$ to excite more resonant modes in the RC and influence the *STN* ratio quality.

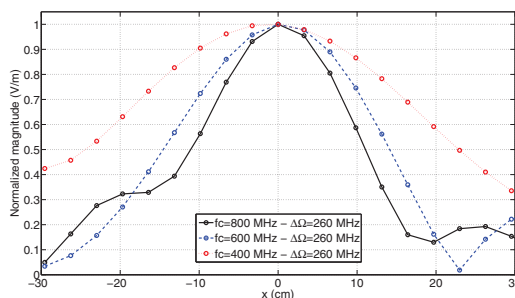


(a)

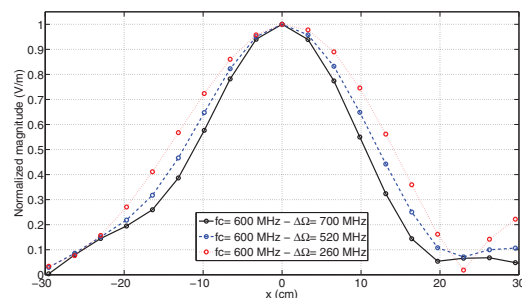


(b)

Fig. 28. (a) Maximum magnitude of focusing. (b) *STN* ratio, importance of focusing from 1 to 20 probes: regarding 50 random draws of probes locations each time (stars markers) and mean trend (plain line).



(a)



(b)

Fig. 29. Normalized total electric field as a function of the distance to R_0 along x : variations around (a) f_c and (b) $\Delta\Omega$.

In the final part of this chapter, the TR is numerically applied in the LASMEA (LABoratoire des Sciences et Matériaux pour l'Électronique et d'Automatique, Clermont Université) MSRC (for impulsive susceptibility test and selective focusing).

6. EMC application and selective focusing

Since 2001, a MSRC has been available for the EMC research & applications of LASMEA. Its dimensions and an internal view are given on Fig. 30. Historically, studies and tests in

the MSRC were made in the frequency domain to provide an internal volume (WV) where the characteristics of the electromagnetic field illuminating the EUT are given with the same probability. A statistically uniform and homogeneous distribution of the electromagnetic field in MSRC means that the same part of energy attacks the EUT from all directions and with all polarizations (when averaged over the number of stirrer positions, i.e. over a full rotation of it). Nevertheless, this means that the illumination is statistically the same for the whole EUT, which can be a disadvantage, especially if the reliability is not the same for all components of the EUT.

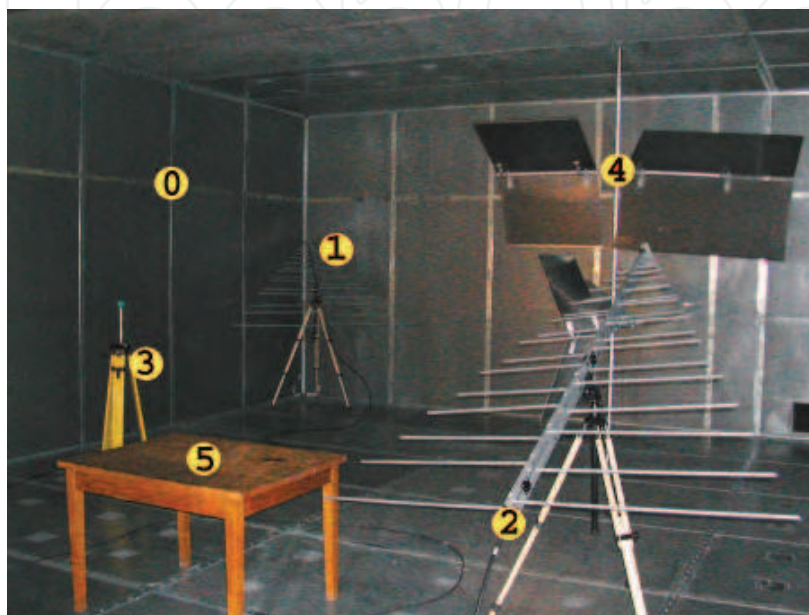


Fig. 30. Inner view of LASMEA MSRC ($6.7 \times 8.4 \times 3.5 \text{ m}^3$). Characteristics: (0) walls, (1) emitting and (2) receiving antennas, (3) field's probe, (4) mechanical stirrer, (5) working volume.

The application of the TR technique allows us to bring time techniques for EMC studies in MSRC. One of these intended applications is the impulsive susceptibility test and selective focusing that will be considered as a solution of the problem described above. To do this, we will use the commercial software CST MICROWAVE STUDIO® to numerically treat this case. In the next section, we will point to this software and the numerical set up used.

6.1 Numerical configuration

CST MICROWAVE STUDIO® is a specialist tool for the 3-D electromagnetic simulation. Inspired by the characteristics of LASMEA MSRC, the Fig. 31 shows the configuration of our example. Simulations are performed with a spatial discretization of 0.65 cm and 4 cm respectively corresponding to the smallest and largest mesh, and a time step of 24.4 ps .

The walls of the MSRC are modeled with a conductivity of $S_c = 1.1 \cdot 10^6 \text{ S/m}$, furthermore the stirrer has a conductivity of $2.74 \cdot 10^7 \text{ S/m}$. The support table and the EUT are made respectively of wood and aluminum ($S_c = 3.56 \cdot 10^7 \text{ S/m}$). In this application, we wish to focus separately on the three components of the EUT modeled by dipoles (1, 2, and 3 in Fig. 31). The excitation signal is a Gaussian modulated sine pattern with a central frequency of 250 MHz and a bandwidth of 300 MHz calculated at -20 dB . The TRM is composed of two 60 cm half-wavelength antennas.

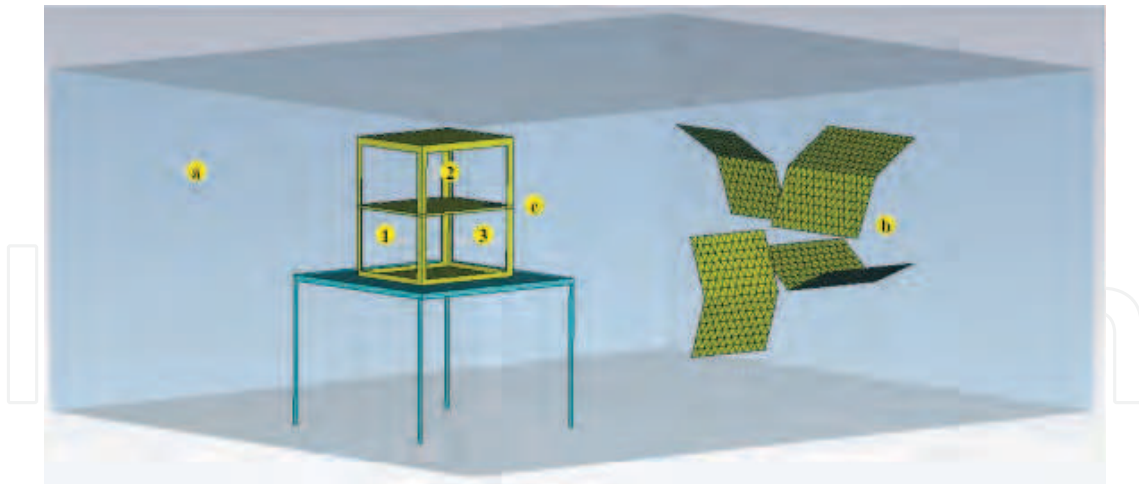


Fig. 31. LASMEA MSRC modeled by CST MICROWAVE STUDIO® : (a) walls, (b) mechanical stirrer, (c) EUT, (1)(2)(3) EUT three components.

6.2 Preliminary study

To justify the choice of the TRM antenna number, the duration of the TR window (Δt), and the ability to choose the polarization of the focused signal, a preliminary study is carried out maintaining the configuration of the Fig. 31 without the table and the EUT; but, here, an isotropic probe will be used to check focusing properties. Based upon TR principles, and because the simulator does not allow exciting probes and there are not designated to broadcast, necessary signals for the second phase of TR may be obtained directly by injecting excitation signal straightforward on the TRM antennas one by one. The three Cartesian components of these impulse responses are recorded by an isotropic field probe, and then back propagated from the TRM. Indeed, during the first phase, the isotropic probe records the electric field E_α (with $\alpha = x, y$ or z : Cartesian component of the field). We can choose the polarization α of the focused signal ($E_{TR\alpha}$) from back-propagating by the TRM recorded signal corresponding either to x, y or z without changing the polarization of the TRM antennas (Fig. 32).

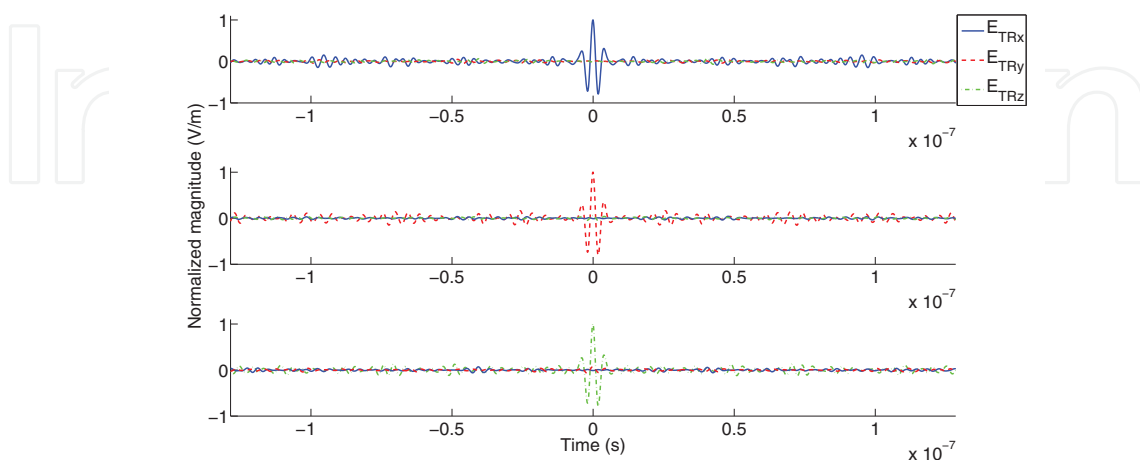


Fig. 32. Polarization control of the focused signal.

To determine the TR window duration (Δt), we need to calculate the Heisenberg time. Thus, we plotted on Fig. 33a the evolution of the *STN* ratio as a function of Δt for a TRM composed of a single antenna. Already mentioned above, we note that the *STN* ratio stabilizes after a certain duration, we can deduce that the Heisenberg time is about $8 \mu s$. However an $8 \mu s$ simulation in comparison with the large dimensions of the LASMEA MSRC is disadvantageous in terms of computing time, so we chose to reduce simulation time by increasing the TRM antenna number. Fig. 33b shows that for $\Delta t = 0.75 \mu s$ the *STN* ratio stabilizes for a number of antenna greater than 8.

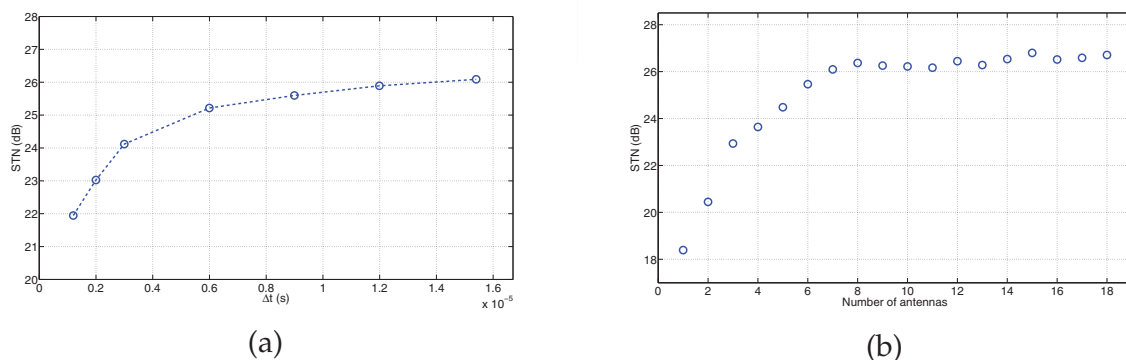


Fig. 33. *STN* ratio evolution: (a) as a function of the TR window for a TRM composed of 1 antenna, (b) as a function of the TRM antenna number with a TR windows of $\Delta t = 0.75 \mu s$.

The number of antennas needed for a TR experience is given by the ratio $\Delta H/\Delta t$, hence we chose the duration $\Delta t = 4 \mu s$ with 2 antennas as TRM.

6.3 Selective focusing

In this section, we will check the possibility to focus the electric field on one of the three components of the EUT, while others are aggressed by lower levels (noise). To do this, we consider the example where the values $15 V/m$, $70 V/m$ and $40 V/m$ correspond respectively to the three components threshold that should not be exceeded by the electric field. After recording the impulse responses $k_{ij}(t)$ with $1 \leq i \leq 2$: number of TRM antennas and $1 \leq j \leq 3$: number of components of the EUT, and given the linearity of the system, we can focus on any component with any desired focusing magnitude by a simple post-processing. Indeed, if for example we want to focus on the component number 2 (Figs. 34c, 34d), we will back-propagate through the first antenna of the TRM the signal $pk_{12}(-t)$ and the signal $pk_{22}(-t)$ by the second antenna, where p is the weight corresponding to the needed amplification. The p coefficient stands for the focusing magnitude control offered by TR (the focusing peak may be increased or decreased throughout the number of TRM antennas, the TR window duration, or an external amplification weight). We plotted in Fig. 34 temporal and spatial focusing corresponding to the "on demand" desired peak magnitude separately on each of the three components. The spatial focusing of the field corresponds to the absolute maximum value recorded over the entire simulation for each cell of the slice plan).

We note that for the different cases, the maximum of the field corresponds to the desired spatial location of each component. In addition, we note that for the second case, for example, we have focused on the component 2 (Figs. 34c, 34d) while respecting the threshold of the first component (component 1 was aggressed by a field whose numerical value is smaller than $15 V/m$), same for the third case. To achieve this desired focusing magnitude on component 2

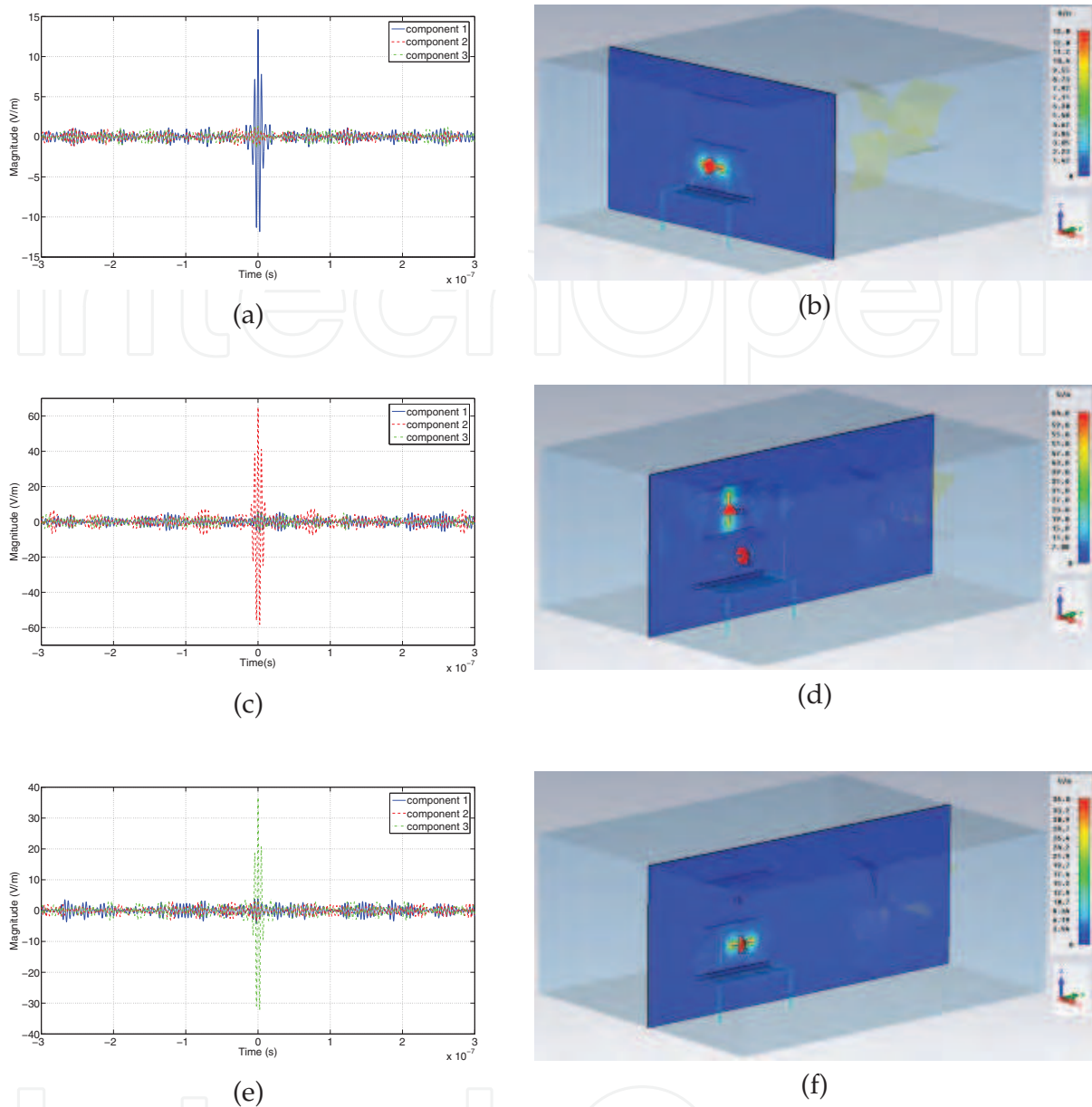


Fig. 34. Temporal focusing of the electric field on: (a) component 1 with $p = 1$, (c) component 2 with $p = 5$, (e) component 3 with $p = 3$. Spatial focusing corresponding to the absolute maximum value of the electric field: (b) component 1 with $p = 1$, (d) component 2 with $p = 5$, (f) component 3 with $p = 3$.

(64 V/m) smaller than the corresponding threshold (70 V/m), the impulse responses $k_{12}(-t)$ and $k_{22}(-t)$ were multiplied by the weight $p = 5$; so we notice that following this way we can control the time, location, and magnitude of focusing (by the weight p).

Finally, if we wish, for example, to focus on the first and third components with respective magnitude of 13 V/m and 35 V/m, we sum and back-propagate the needed impulse responses (on the first TRM antenna we back-propagate the signal $p_1 k_{11}(-t) + p_3 k_{13}(-t)$ with $p_1 = 1$ and $p_3 = 3$, on the second TRM antenna we back-propagate the signal $p_1 k_{21}(-t) + p_3 k_{23}(-t)$). The Fig. 35 justifies this approach and shows the ability of selective focusing by TR.

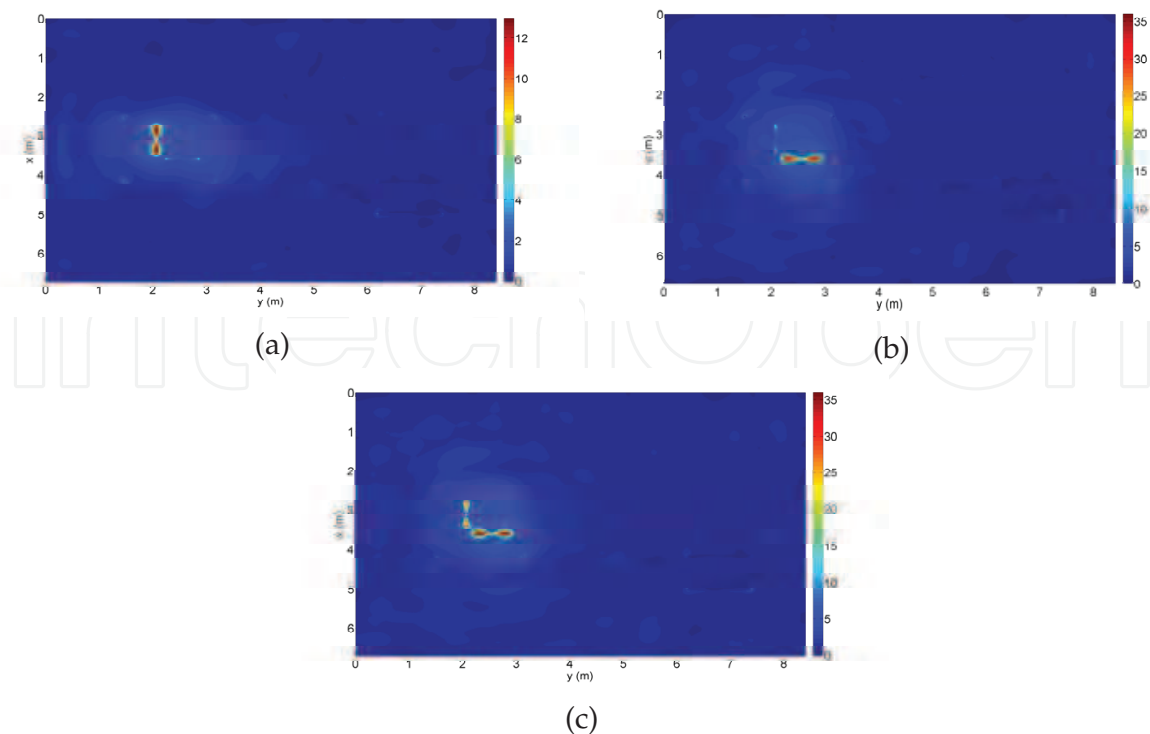


Fig. 35. Cutting plan ($z = 1.4 \text{ m}$) of the absolute maximum value of the electric field obtained on the: (a) component 1 with $p = 1$, (b) component 3 with $p = 3$, (c) two components together, 1 with $p = 1$ and 3 with $p = 3$.

7. Conclusions

In this chapter, the TR method was presented in electromagnetism for applications concerning the EMC domain in a reverberating environment. Based upon the equivalence between backward propagation and reversibility of the wave equation, many TR experiments were led successfully in acoustics. In this chapter, after an introduction explaining the physical context, the theoretical principles of TR were described and illustrated numerically using the FDTD method. The use of the CST MICROWAVE STUDIO® commercial software laid emphasis on the industrial interest of TR for EMC test devices. First, the TR technique was applied in free space using a TRC and a TRM, and then the importance of the complexity of the medium was demonstrated. Relying on intrinsic RC behavior and due to multiple reflections, the results obtained by applying TR in a reverberating cavity were clearly improved; the aim was to accurately describe the influence of various parameters above focusing. Thus, a link between the modal density in a cavity and the TR focusing quality was clearly established through the STN ratio. A particular interest relies on the number and locations of TR probes and the excitation pulse parameters impact. Finally we introduced an original way to perform an impulsive susceptibility test study based on the MSRC use. We presented the possibility to choose the polarization of the wave aggressing the EUT, and to perform an "on demand" selective focusing. In further works, it would be interesting to experimentally confirm our numerical results, so one may expect to proceed to experimental analysis in LASMEA MSRC. At last, considering the characteristics of EMC applications in MSRC, a closer look might be set to the advantages of TR numerical tools for innovating studies in reverberation chambers.

8. References

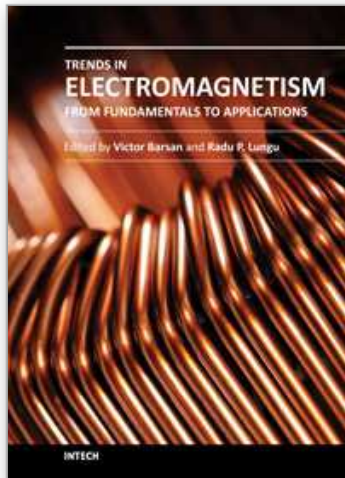
- Bonnet, P.; Vernet, R.; Girard, S. & Paladian, F. (2005). FDTD modelling of reverberation chamber, *Electronics Letters*, Vol. 41, No. 20, 2005, 1101-1102, ISSN 0013-5194.
- Corona, P.; Ladbury, J. & Latmiral, G. (2002). Reverberation-chamber research - then and now: A review of early work and comparison with current understanding, *IEEE Transactions on Electromagnetic Compatibility*, Vol. 44, No. 1, 2002, 87-94, ISSN 0018-9375.
- Cozza, A. & Moussa, H. (2009). Enforcing deterministic polarization in a reverberating environment, *Electronics Letters*, Vol. 45, No. 25, 2009, ISSN 0013-5194.
- Davy, M.; de Rosny, J. & Fink, M. (2009). Focalisation et amplification d'ondes électromagnétiques par retournement temporel dans une chambre réverbérante, *Journées scientifiques d'URSI, Propagation et Télédétection*, pp. 13-20, France, 2009.
- de Rosny, J. (2000). *Milieux réverbérants et réversibilité*, PhD thesis, Paris VI - Pierre et Marie CURIE University, 2000.
- de Rosny, J. & Fink, M. (2002). Overcoming the diffraction limit in wave physics using a time-reversal mirror and a novel acoustic sink, *Physical Review Letters*, Vol. 89, No. 12, 2002, ISSN 1079-7114.
- de Rosny, J.; Lerosey, G.; Tourin, A. & Fink, M. (2007). Time reversal of electromagnetic waves, *Modeling and computations in electromagnetics*, Springer Berlin Heidelberg, Vol. 59, 2007, 187-202, ISBN 3540737774.
- Derode, A.; Tourin, A. & Fink, M. (1999). Ultrasonic pulse compression with one-bit time reversal through multiple scattering, *Journal of Applied Physics*, Vol. 85, No. 9, 1999, 6343-6352, ISSN 0021-8979.
- Derode, A.; Tourin, A.; de Rosny, J.; Tanter, M.; Yon, S. & Fink, M. (2003). Taking advantage of multiple scattering to communicate with time-reversal antennas, *Physical Review Letters*, Vol. 90, No. 1, 2003, ISSN 1079-7114.
- Directive 89/336/CEE (1989). Guide d'application de la Directive 89/336/CEE du Conseil du 3 mai 1989 concernant le rapprochement des législations des États membres relatives à la compatibilité électromagnétique. URL: [http : //cmrt.centrale – marseille.fr/electromagnetisme/veille/guide89336.pdf](http://cmrt.centrale-marseille.fr/electromagnetisme/veille/guide89336.pdf)
- Edelmann, G. F. (2005). An overview of time-reversal acoustic communications, *Proceedings of TICA 2005*, 2005.
- El Baba, I.; Lalléchère, S. & Bonnet, P. (2009). Electromagnetic time-reversal for reverberation chamber applications using FDTD, *Proceedings of ACTEA 2009, International Conference on Advances in Computational Tools for Engineering Applications*, pp. 157-167, ISBN: 978-1-4244-3833-4, Lebanon, 2009.
- El Baba, I.; Patier, L., Lalléchère, S. & Bonnet, P. (2010). Numerical contribution for time reversal process in reverberation chamber, *Proceedings of APS-URSI 2010, IEEE Antennas and Propagation Society International Symposium*, ISBN: 978-1-4244-4967-5, Canada, 2010.
- Emerson, W. (1973). Electromagnetic wave absorbers and anechoic chambers through the years, *IEEE Transactions on Antennas and Propagation*, Vol. 21, No. 4, 1973, 484-490, ISSN 0018-926X.
- Fink, M. (1992). Time reversal of ultrasonic fields - Part I: Basic principles, *IEEE Transactions on Ultrasonics, Ferroelectrics, and Frequency Control*, Vol. 39, No. 5, 1992, 555-566, ISSN 0885-3010.

- Hill, D.A. (1998). Plane wave integral representation for fields in reverberation chambers, *IEEE Transactions on Electromagnetic Compatibility*, Vol. 40, No. 3, 1998, 209-217, ISSN 0018-9375.
- Jackson, J.D. (1998). *Classical Electrodynamics Third Edition*, John Wiley and Sons Inc, 1998.
- Lerosey, G.; de Rosny, J.; Tourin, A.; Derode, A.; Montaldo, G. & Fink, M. (2004). Time reversal of electromagnetic waves, *Physical Review Letters*, Vol. 92, No. 19, 2004, ISSN 1079-7114.
- Liu, B.H & Chang, D.C (1983). Eigenmodes and the composite quality factor of a reverberating chamber, *National Bureau of Standards, USA, Technical Note*, 1983.
- Liu, D.; Kang, G.; Li, L.; Chen, Y.; Vasudevan, S.; Joines, W.; Liu, Q.H.; Krolik, J. & Carin, L. (2005). Electromagnetic time-reversal imaging of a target in a cluttered environment, *IEEE Transactions on Antennas and Propagation*, Vol. 53, No. 9, 2005, 3058-3066, ISSN 0018-926X.
- Maaref, N.; Millot, P. & Ferrières, X. (2008). Electromagnetic imaging method based on time reversal processing applied to through-the-wall target localization, *Progress In Electromagnetics Research M*, Vol. 1, 2008, 59-67, ISSN 1937-8726.
- Moussa, H.; Cozza, A. & Cauterman, M. (2009a). A novel way of using reverberation chambers through time-reversal, *Proceedings of ESA 2009, ESA Workshop on Aerospace EMC, Italy*, 2009.
- Moussa, H.; Cozza, A. & Cauterman, M. (2009b). Directive wavefronts inside a time reversal electromagnetic chamber, *Proceedings of EMC 2009, IEEE International Symposium on Electromagnetic Compatibility*, pp. 159-164, ISBN: 978-1-4244-4266-9, USA, 2009.
- Mur, G. (1981). Absorbing boundary conditions for the finite-difference approximation of the time-domain electromagnetic-field equations, *IEEE Transactions on Electromagnetic Compatibility*, Vol. EMC-23, No. 4, 1981, 377-382, ISSN 0018-9375.
- Neyrat, M.; Guiffaut, C. & Reineix, A. (2008). Reverse time migration algorithm for detection of buried objects in time domain, *Proceedings of APS 2008, IEEE Antennas and Propagation Society International symposium*, ISBN: 978-1-4244-2041-4, USA, 2008.
- Neyrat, M. (2009). *Contribution à l'étude de G.P.R. (Ground Penetrating Radar) multicapteurs. Méthodes directes et inverses en temporel*, PhD thesis, Limoges University, 2009.
- Prada, C. & Fink, M. (1994). Eigenmodes of the time reversal operator: A solution to selective focusing in multiple-target media, *Wave Motion, Elsevier, Kidlington*, Vol. 20, No. 2, 1994, 151-163, ISSN 0165-2125.
- Quieffin, N. (2004). *Etude du rayonnement acoustique de structures solides : vers un système d'imagerie haute résolution*, PhD thesis, Paris VI - Pierre et Marie CURIE University, 2004.
- Sorrentino, R.; Roselli, L. & Mezzanotte, P. (1993). Time reversal in finite difference time domain method, *IEEE Microwave and Guided Wave Letters*, Vol. 3, No. 11, 1993, 402-404, ISSN 1051-8207.
- Yavuz, M. & Teixeira, F. (2006). Full time-domain DORT for ultrawideband electromagnetic fields in dispersive, random inhomogeneous media, *IEEE Transactions on Antennas and Propagations*, Vol. 54, No. 8, 2006, 2305-2315, ISSN 0018-926X.
- Yee, K. S. (1966). Numerical solution of initial boundary value problems involving Maxwell's equations in isotropic media, *IEEE Transactions on Antennas and Propagation*, Vol. Ap-14, No. 3, 1966, 302-307, ISSN 0018-926X.

Ziadé, Y.; Wong, M. & Wiart, J. (2008). Reverberation chamber and indoor measurements for time reversal application, *Proceedings of APS 2008, IEEE Antennas and Propagation Society International Symposium*, ISBN: 978-1-4244-2041-4, USA, 2008.

IntechOpen

IntechOpen



Trends in Electromagnetism - From Fundamentals to Applications

Edited by Dr. Victor Barsan

ISBN 978-953-51-0267-0

Hard cover, 290 pages

Publisher InTech

Published online 23, March, 2012

Published in print edition March, 2012

Among the branches of classical physics, electromagnetism is the domain which experiences the most spectacular development, both in its fundamental and practical aspects. The quantum corrections which generate non-linear terms of the standard Maxwell equations, their specific form in curved spaces, whose predictions can be confronted with the cosmic polarization rotation, or the topological model of electromagnetism, constructed with electromagnetic knots, are significant examples of recent theoretical developments. The similarities of the Sturm-Liouville problems in electromagnetism and quantum mechanics make possible deep analogies between the wave propagation in waveguides, ballistic electron movement in mesoscopic conductors and light propagation on optical fibers, facilitating a better understanding of these topics and fostering the transfer of techniques and results from one domain to another. Industrial applications, like magnetic refrigeration at room temperature or use of metamaterials for antenna couplers and covers, are of utmost practical interest. So, this book offers an interesting and useful reading for a broad category of specialists.

How to reference

In order to correctly reference this scholarly work, feel free to copy and paste the following:

Ibrahim El Baba, Sébastien Lalléchère and Pierre Bonnet (2012). Time Reversal for Electromagnetism: Applications in Electromagnetic Compatibility, Trends in Electromagnetism - From Fundamentals to Applications, Dr. Victor Barsan (Ed.), ISBN: 978-953-51-0267-0, InTech, Available from: <http://www.intechopen.com/books/trends-in-electromagnetism-from-fundamentals-to-applications/time-reversal-for-electromagnetism-applications-in-electromagnetic-compatibility>

INTECH
open science | open minds

InTech Europe

University Campus STeP Ri
Slavka Krautzeka 83/A
51000 Rijeka, Croatia
Phone: +385 (51) 770 447
Fax: +385 (51) 686 166
www.intechopen.com

InTech China

Unit 405, Office Block, Hotel Equatorial Shanghai
No.65, Yan An Road (West), Shanghai, 200040, China
中国上海市延安西路65号上海国际贵都大饭店办公楼405单元
Phone: +86-21-62489820
Fax: +86-21-62489821

© 2012 The Author(s). Licensee IntechOpen. This is an open access article distributed under the terms of the [Creative Commons Attribution 3.0 License](#), which permits unrestricted use, distribution, and reproduction in any medium, provided the original work is properly cited.

IntechOpen

IntechOpen